

Project Number: CHE-JW1-8298

DESIGN OF A MULTI-POLLUTANT SORBENT FOR COAL GASIFICATION

A Major Qualifying Project Report:
submitted to the Faculty
of the
WORCESTER POLYTECHNIC INSTITUTE
in partial fulfillment of the requirements for the
Degree of Bachelor of Science

by

Catherine Casey

Katie Hudon

Elizabeth J. Stewart
Date: April 17, 2008

Approved:

Professor Jennifer Wilcox, Advisor

ABSTRACT

The capture of trace elements in coal gasification and combustion is an important environmental issue. The binding of trace element species of Hg, As, and Se were investigated with several metal dimers, Au, Pd, Pt, V, Fe, and Cu using *ab initio*-based methods. The Fe dimer had the most favorable (≥ 50 kcal/mol) binding energies. A detailed orbital analysis was used to study the binding with Fe. In the reactions considered, Fe was the electron donor and has the prospect to be a multi-pollutant sorbent for coal-based energy generation applications.

EXECUTIVE SUMMARY

In the past few years, the impact of power generation on the environment has been brought into the front light. Coal combustion is the major energy producer in the US, but it is not environmentally sound. Coal combustion releases many pollutants into the atmosphere, including SO_x , NO_x , and trace elements such as mercury (Hg), selenium (Se), and arsenic (As). Coal gasification is another method of producing energy from coal, and is more efficient than coal combustion. Integrated Gasification Combined Cycle (IGCC) is the process that uses coal gasification gas turbines along with steam turbines to produce energy. Since the operating conditions are different from coal combustion, the speciation of trace elements is also different. The major species found in coal gasification flue gas are Hg, H_2Se , As, and As_2 .

The goal of this MQP was to design a multi-pollutant sorbent for the application of both coal combustion and gasification. Several metals, in the form of dimers, were studied to find the best candidate for the sorbent; these metals included Au, Pd, Pt, V, Fe, and Cu. The Gaussian software package was employed for the calculations using *ab initio*-based methods to predict the binding energies of the trace element species with the metal dimers. First the best level of theory was determined for each atom from comparisons with experimental values. The best levels of theory were found to be B3LYP/ECP60MDF for Hg, B3LYP/6-311G* for As, Se, and S, B3LYP/1992 for gold (Au), palladium (Pd), platinum (Pt), vanadium (V), copper (Cu), and B3LYP/LANL2DZ for iron (Fe).

Next, the binding energies for all combinations of trace element species with each metal dimer were calculated. The most favorable binding energies of 50 kcal/mol and

above (known as strong chemisorptions), were observed when Fe was the sorbent. Iron is also the one of the most economical materials compared to the other sorbents considered in this project. Some practical considerations may limit the use of pure bulk Fe as a sorbent material since it can easily undergo oxidation reactions which can inhibit its adsorption abilities. An alternative is to alloy Fe with another material such as Cu. In this way, the strong chemisorption properties of Fe will be retained but the new material may be less reactive toward oxidation. However, coal gasification takes place in a reducing environment, so most likely oxidation will not be a concern. The combustion environment is oxidizing so that this material might not be appropriate for combustion applications.

Since Fe appears to have the best possibility for use as a multi-pollutant sorbent for coal gasification, HOMO/LUMO maps and energy differences (ΔE_{HL} 's) were created for Fe with the most abundant trace element species. It was determined from the orbital analysis that Fe atoms donate their electrons to the trace element species. However, a significant amount of electron density remains with the Fe atoms following binding. This indicates that Fe could possibly capture more than one pollutant because this same site of electron density could be reactive with multiple pollutants. All of these factors are very important to the design of a multi-pollutant sorbent for coal gasification.

ACKNOWLEDGEMENTS

We would like to take this time to thank the people who advised us throughout this project.

Professor Jennifer Wilcox, WPI, Project Advisor

Erdem Sasmaz, WPI Graduate Student

Dr. Shela Aboud, Senior Research Associate, Stanford University

TABLE OF CONTENTS

ABSTRACT.....	2
EXECUTIVE SUMMARY	3
ACKNOWLEDGEMENTS	5
TABLE OF CONTENTS.....	6
TABLE OF FIGURES	8
LIST OF TABLES	9
CHAPTER 1: INTRODUCTION.....	10
CHAPTER 2: BACKGROUND	12
2.1 Coal Consumption	12
2.2 Coal Gasification	14
2.2.1 Gasification Speciation	19
2.2.2 IGCC Projects	21
2.3 Trace Element Emissions.....	23
2.3.1 Mercury.....	23
2.3.2 Arsenic	25
2.3.3 Selenium	26
2.4 Current Trace Element Removal Practices	28
2.5 Sorbent Materials	29
2.5.1 Gold.....	29
2.5.2 Palladium	30
2.5.3 Platinum	31
2.5.4 Vanadium.....	32
2.5.5 Iron.....	33
2.5.6 Copper.....	34
2.5.7 Cost Comparison of Sorbent Materials.....	35
2.6 Computational Chemistry	36
2.7 Summary	38
CHAPTER 3: METHODOLOGY	39
3.1 Level of Theory Justification	40
3.2 Ground-State Multiplicities	40
3.3 Orientation of Reactions	41
3.4 Binding Energy	41
3.5 HOMO and LUMO Maps.....	42
3.6 Orbital Analysis	43
3.7 Summary	44
CHAPTER 4: RESULTS & DISCUSSION	45
4.1 Level of Theory Justification	45
4.2 Binding Energies.....	47
4.2.1 Characterization of Binding Energies.....	47
4.2.2 Ground-State Binding Energies of Trace Element Species on Metal Dimers	47
4.3 Orbital Analysis of Fe ₂	51
4.3.1 Fe ₂ + Hg	52
4.3.2 Fe ₂ + H ₂ Se	53
4.3.3 Fe ₂ + As.....	54
4.3.4 Fe ₂ + As ₂	56
4.3.5 Summary of the Orbital Analysis	57
4.4 Sources of Error	58
4.5 Summary of Results and Discussion.....	59

CHAPTER 5: CONCLUSIONS	60
CHAPTER 6: RECOMMENDATIONS AND FUTURE RESEARCH	62
APPENDIX.....	64

TABLE OF FIGURES

Figure 1: Schematic of IGCC Process	14
Figure 2: Fixed-Bed Gasifier	16
Figure 3: Fluidized Bed Gasifier	17
Figure 4: Entrained Flow Gasifier	18
Figure 5: Comparison of Three Main Types of Gasifiers	19
Figure 6: Equilibrium Speciation of Mercury.....	20
Figure 7: Equilibrium Speciation of Arsenic	20
Figure 8: Equilibrium Speciation of Selenium	21
Figure 9: Polk Power Station	22
Figure 10: Wabash Power Station	22
Figure 11: Binding Energies of Trace Element Species on Metal Dimers	49
Figure 12: Orbital Analysis of $\text{Fe}_2 + \text{Hg} \rightarrow \text{Fe}_2\text{Hg}$	53
Figure 13: Orbital Analysis of $\text{Fe}_2 + \text{H}_2\text{Se} \rightarrow \text{H}_2\text{SeFe}_2$	54
Figure 14: Orbital Analysis of $\text{Fe}_2 + \text{As} \rightarrow \text{Fe}_2\text{As}$	55
Figure 15: Orbital Analysis of $\text{Fe}_2 + \text{As}_2 \rightarrow \text{Fe}_2\text{As}_2$	57

LIST OF TABLES

Table 1: United States Mercury Emissions.....	13
Table 2: Toxicity of Mercuric Species.....	24
Table 3: Toxicity of Arsenic Species ²⁷	26
Table 4: Toxicity of Selenium Species.....	27
Table 5: Surface Area of Support Materials.....	31
Table 6: Cost Comparison of Sorbent Materials.....	35
Table 7: Summary of Methodology.....	39
Table 8: Experimental and Calculated Dimer Vibrational Frequencies.....	46
Table 9: Experimental and Calculated Dimer Bond Lengths.....	46
Table 10: Experimental and Calculated Fe ₂ Vibrational Frequencies and Bond Lengths.....	46
Table 11: Level of Theory Chosen for Each Element.....	46
Table 12: Types of Adsorption.....	47
Table 13: Fe Binding Energy Trend from Highest BE to Lowest BE.....	49
Table 14: Multiplicities and Binding Energies of Fe ₂ Reactions.....	64
Table 15: Multiplicities and Binding Energies of Au ₂ Reactions.....	65
Table 16: Multiplicities and Binding Energies of Pd ₂ Reactions.....	66
Table 17: Multiplicities and Binding Energies of Pt ₂ Reactions.....	67
Table 18: Multiplicities and Binding Energies of V ₂ Reactions.....	68
Table 19: Multiplicities and Binding Energies of Cu ₂ Reactions.....	69
Table 20: HOMO/ LUMO ΔE_{HL} 's of Fe ₂ + Hg \rightarrow Fe ₂ Hg.....	69
Table 21: HOMO/ LUMO ΔE_{HL} 's of Fe ₂ + H ₂ Se \rightarrow H ₂ SeFe ₂	70
Table 22: HOMO/ LUMO ΔE_{HL} 's of Fe ₂ + As \rightarrow Fe ₂ As.....	70
Table 23: HOMO/ LUMO ΔE_{HL} 's of Fe ₂ + As ₂ \rightarrow Fe ₂ As ₂	70

CHAPTER 1: INTRODUCTION

Utilizing coal to supply energy leads to the release of pollutants such as NO_x, SO_x, CO₂, and trace elements (mercury(Hg), arsenic(As) and selenium(Se)) into the environment. Currently, of the three main locations (China, United States, and India) with recoverable coal reserves, the U.S. is leading the effort to decrease harmful emissions into the environment, through regulations such as the EPA's Clean Air Interstate Rule (CAIR), which places caps on NO_x and SO_x emissions from the Eastern states, and the Clean Air Mercury Rule, which places a cap on Hg emissions from coal-fired power plants.⁴ In the United States, annual energy use from coal is projected to increase from 22.9×10^{15} Btu in 2005 to 34.1×10^{15} Btu in 2030.¹ This research aims to design a multi-pollutant sorbent to remove Hg, As, and Se from the high temperature environment of coal gasification.

The background section of this Major Qualifying Project (MQP) report describes: a) the scope of present and future coal consumption, b) an overview of coal gasification, c) the trace elements of interest for removal (Hg, As, Se), d) current trace element removal practices, e) justification for each sorbent material choice (Pd₂, Au₂, Pt₂, V₂, Cu₂, and Fe₂), and f) an overview of the computational chemistry techniques employed. These sections are described to provide the rationale for the reactions analyzed.

The methodology section provides: a) the basis set justification, b) the method for determining the ground state of each reaction, c) methods for choosing the orientation of each reaction, d) the procedure for finding binding energies of reactions, and e) an overview of Highest Occupied Molecular Orbital (HOMO)/ Lowest Unoccupied Molecular Orbital (LUMO) analysis.

The results presented in this MQP include a discussion of: a) the basis sets chosen, b) the ground state binding energies for each reaction analyzed, and c) the orbital analysis for the most promising reactions.

Through the calculations and investigations carried out in this Major Qualifying Project the following objectives have been met: a) the determination of the adsorption energetics of various Hg species (Hg, HgH, HgS), As species (As₂, AsS, AsH, AsH₃, As), Se species (Se, H₂Se, HSe, SeS), and H₂S, i.e., typical trace elements indicative of a reducing gasification environment, with dimers of Pd₂, Au₂, Pt₂, V₂, Cu₂, and Fe₂ using density functional theory and relativistic effective core potentials for the heavier atoms, b) the evaluation of the effectiveness of each metal dimer for the binding of multiple flue gas components, c) the generation of HOMO/LUMO maps for understanding the chemistry of the reactions, d) the orbital analysis for reactions involving Fe and Hg, H₂Se, As, and As₂, and e) the recommendations for the use of Pd, Au, Pt, V, Cu, and Fe as potential catalyst materials for the adsorption of Hg, As, and Se species from the high temperature environment of coal gasification.

CHAPTER 2: BACKGROUND

This section provides background information on coal consumption, coal gasification, trace element species (Hg, As, Se, and H₂S) and sorbent materials of interest (Pd, Au, Pt, V, Cu, and Fe), and an overview of the computational chemistry techniques employed. This information is provided to place this MQP in the context of current environmental practices and to explain the significance of computational chemistry within these applications.

2.1 Coal Consumption

Fossil fuels are the source of 80% of the world's energy, with twenty-four percent of this energy derived from coal.² The three locations with the highest recoverable coal reserves are the United States with 27% of the world's recoverable reserves, China with 13%, and India with 10%.³

Currently, within the United States, 50% of electricity is produced from coal, and there are over five hundred 500-megawatt coal-fired power plants in the country. In China, every week there are two new 500-megawatt coal-fired power plants constructed to provide both electricity and industrial energy.² Also, over 50% of India's energy is derived from coal. The amount of energy produced from coal is predicted to increase 3% by 2030²; China and India account for 68% of this projected increase in coal consumption.²

Of the three locations with recoverable coal reserves, the U.S. is leading the effort to decrease harmful emissions into the environment through regulations such as the EPA's Clean Air Interstate Rule (CAIR), which placed caps on NO_x and SO_x emissions from the Eastern states, the Clean Air Mercury Rule (CAMR), which places

a cap on Hg emissions from coal-fired power plants⁴, and the Supreme Court ruling on April 2, 2007 that authorized the EPA to regulate greenhouse gas emissions from automobiles.⁵ On February 8, 2008, the DC Circuit Court vacated the CAMR, however, the EPA is in the process of evaluating the impact of this decision⁴. However, the release of emissions from coal-fired power plants is a global problem, and solutions for capturing CO₂, SO_x, NO_x, Hg, As and Se should be implemented in both the developed and developing world.

The Clean Air Mercury Rule (CAMR) is important to the present work. CAMR was established by the EPA in 2005 to place a cap on Hg emissions from coal-fired power plants in two phases, as depicted in *Table 1*. The first cap is to be implemented in 2010 and caps emissions at 38 tons/ year. The second cap will be enforced in 2018 and reduced emissions to 15 tons/year of Hg emissions. Currently within the United States, 50 tons Hg/year are emitted, and globally there are 5,000 tons Hg/ year emitted.

United States	Hg Emissions (tons/yr)
Present Emissions	50
CAMR First Phase Cap (2010)	38
CAMR Second Phase Cap (2018)	15

Table 1: United States Mercury Emissions

As coal consumption increases worldwide the need for sorbent materials to capture harmful components of flue gases before being released into the environment becomes of increased importance. This work specifically focuses on the removal of Hg, As, Se, and H₂S from the flue gases produced from coal-fired power plants.

2.2 Coal Gasification

Coal gasification was developed in the 1970's. The rise of natural gas prices launched coal as a major source of power. Also, the emerging environmental considerations for acid rain adjusted the objectives of power stations to include SO_x and NO_x emissions, which inspired the advancement of a new coal power technology, Integrated Gasification Combined Cycle (IGCC).⁶

IGCC is a power cycle that has two major power generating steps. First, coal is gasified to produce a synthesis gas (syngas), mostly made of H_2 and CO . This syngas is then sent through a gas turbine where energy is harvested. In the following step, a heat recovery steam generator (HRSG) is used to transfer heat (energy) from the syngas to steam. The hot steam is then passed through a steam turbine where even more energy is collected. See *Figure 1* for a general schematic of an IGCC plant. Since the pollutants can be separated before combustion takes place, it is possible to achieve lower emissions. The double turbines and low emissions make IGCC plants very appealing to the power generation industry.⁶

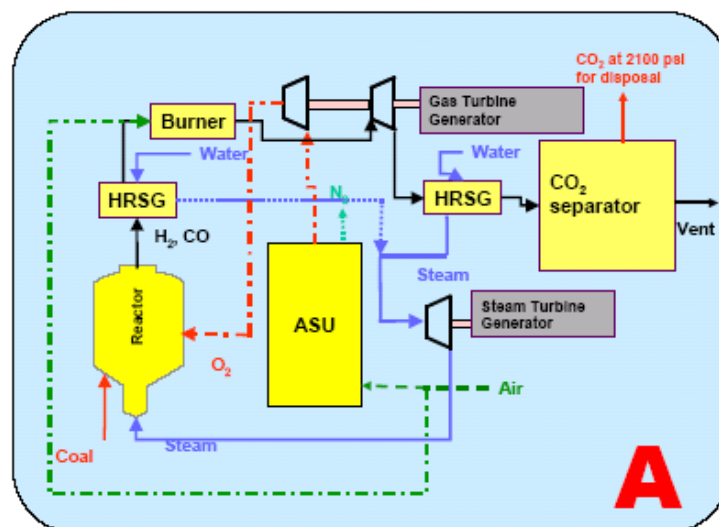
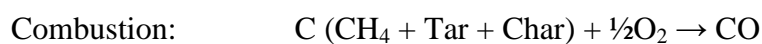
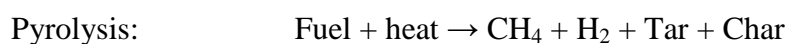


Figure 1: Schematic of IGCC Process⁷

Gasification is the process of converting carbon-containing material to H₂ and CO, by reacting the material with a strictly-controlled amount of O₂ at elevated temperatures. Pyrolysis is the first step, which is to heat the material to a very high temperature, where tars (pollutants) are volatilized and the mass of char that is left is then passed onto the combustion reaction. In the combustion reaction oxygen (or air) is fed and reacted with the char giving CO and CO₂ as products, as well as heat and energy for the gasification reaction. The gasification reaction includes steam and CO₂ reacting with the char to produce the H₂ and CO in a reducing environment.⁸ The water-gas shift reaction is also present and reaches equilibrium at the given conditions.



Types of gasification reactors include fixed-bed, fluidized-bed, and entrained-flow. A fixed-bed gasifier (*Figure 2*) can either be in a counter-current or co-current configuration. In both, a stream of steam and oxygen (or air) flows through a bed of fuel. The fuel used must not cake, so it can remain permeable to the stream of gas. The overall efficiency is lower than that for a fluidized bed. In the counter-current configuration, methane (CH₄) and tar levels are relatively high in the outlet gas stream; therefore, it must be cleaned thoroughly before being sent to the turbine or recycled back to the reactor. However, in the co-current configuration, the gas passes through the hot bed and the tar levels are significantly lower than in the counter-current configuration.⁹

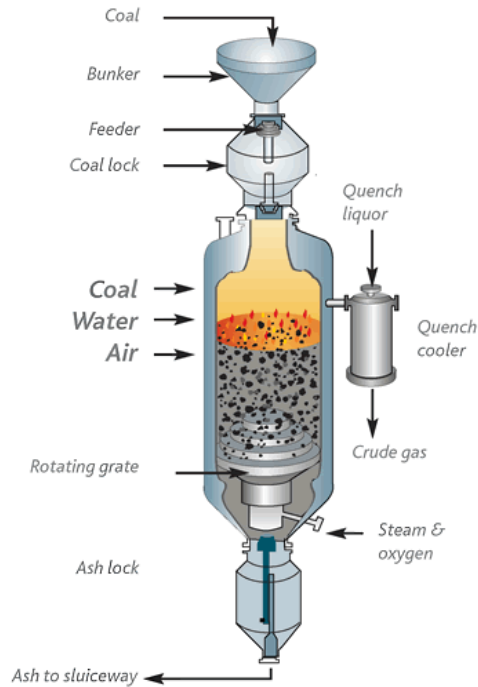


Figure 2: Fixed-Bed Gasifier¹⁰

A fluidized-bed gasifier (*Figure 3*) is used primarily for fuels that have highly corrosive ash, such as biomass fuels. The corrosive ash could damage the walls of the gasifier since it tends to allow a lot of slagging. The coal is fluidized in oxygen (or air) and steam in the reactor. If a low-rank coal is available, the ash is removed in a dry setting allowing the operating temperatures to be lower. On the other hand, if a high-rank coal is used, the ash is collected as agglomerates, which causes the operating temperatures to be somewhat higher. The conversion efficiency is lower than that of the entrained-flow gasifier, but recycling and combustion of solids can help increase the efficiency.⁹

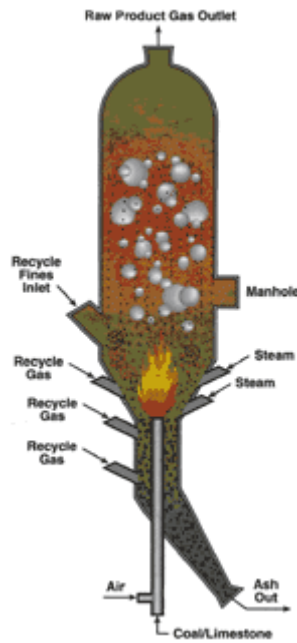


Figure 3: Fluidized Bed Gasifier ¹¹

The entrained-flow is the most popular type of gasifier (*Figure 4*). Pulverized solid and liquid fuel slurry are reacted with oxygen (rarely air) using a co-current configuration. Most ranks of coal are appropriate to use in this type of gasifier because of the very high operating temperatures. These temperatures are well above the ash fusion temperature so the control of slagging is a crucial component of the gasifier's operation. Even though more energy is required to cool the syngas stream after the gasifier, an entrained flow unit has a high efficiency.⁹

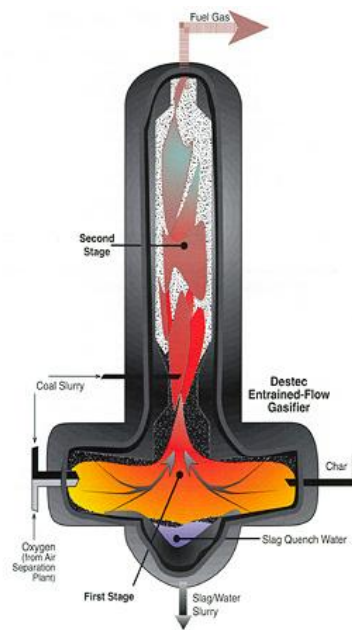


Figure 4: Entrained Flow Gasifier ¹²

Specifically, the Koppers-Totzek method is used in an entrained-flow gasifier. The temperature at the burner of this type of entrained-flow gasifier is around 3500°C. In the main reactor compartment the endothermic reactions that are taking place cause the temperature to drop to about 1700°C. Once the syngas is released it is quenched with water to cool it to 900°C. It is important to note that even cooled syngas has a very high temperature.¹³

The operating conditions for the three types of gasifiers vary slightly. The operating temperature range of the gasifier unit is 800 to 1900°C and the operating pressures are between 10 and 100 bar. These operating conditions allow for the differences between coal combustion and coal gasification to become significant. Coal combustion occurs at a much lower temperature than gasification (200-300°C), with the temperature difference greatly affecting the speciation of trace elements in the unit operation. In fixed-bed gasifiers, the coal particles are larger in comparison to fluidized-bed gasifiers. This difference (about 25 mm) in particle size helps to optimize the mass

transfer in the system. Both fixed- and fluidized-beds operate in similar conditions of 800-1100°C and 10-100 bar. Entrained-flow gasifiers operate at a much higher temperature (1500-1900°C) and require significantly smaller particle size (roughly 0.1 mm) for the coal feed, yet they are still the most popular type of gasifiers due to their relatively high efficiencies. *Figure 5* shows a general comparison of all three types of gasifiers.

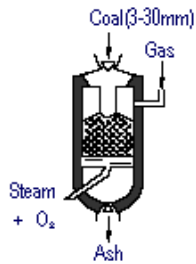
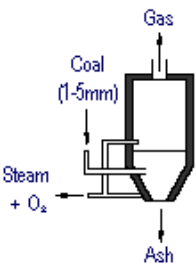
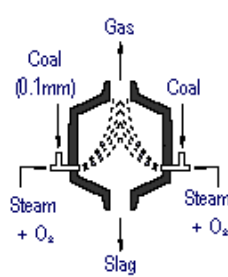
Fixed-Bed	Fluidized-Bed	Entrained-Flow
800-1000 C	800-1100 C	1500-1900 C
10-100 bar	10-25 bar	25-40 bar
		

Figure 5: Comparison of Three Main Types of Gasifiers ¹⁴

2.2.1 Gasification Speciation

In coal gasification, the operating conditions are different from traditional coal combustion; therefore, several trace elements are present in different forms. This is important when examining the trace element emissions that occur in coal gasification plants. A trace element present in the temperature range of 500 – 650 °C and the pressure range of 150-300 psi can pass through the process and be released into the environment.¹⁵ In the case of mercury, coal combustion and coal gasification have the same speciation profile with elemental mercury (Hg^0) as the dominant species¹⁵. Other species present in coal gasification are HgS and HgO , but these species are less prevalent as seen in *Figure 6*. Arsenic oxide (AsO) is the most abundant species at

coal gasification conditions, followed by arsenic sulfide (AsS) and arsine (AsH_3) shown in *Figure 7*. Selenium is most likely in the form selenium hydride (hydrogen selenide, H_2Se).¹⁵ *Figure 8* shows additional selenium species (Se , Se_2 , and SeO) that are also present in coal gasification conditions. Each species has its own characteristics, which are crucial in the study of how to capture them.

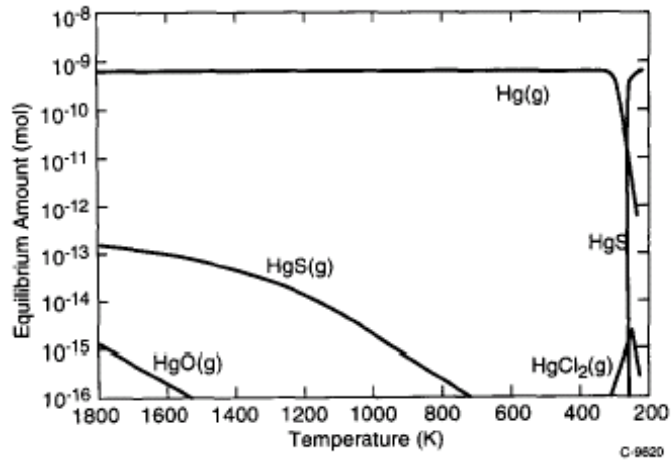


Figure 6: Equilibrium Speciation of Mercury¹⁵

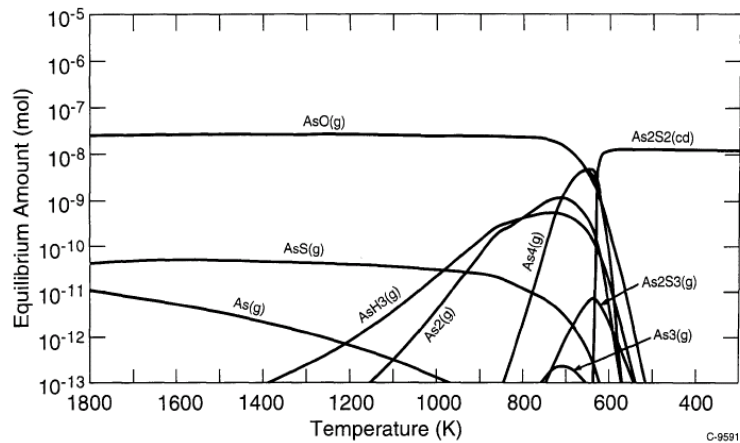


Figure 7: Equilibrium Speciation of Arsenic¹⁵

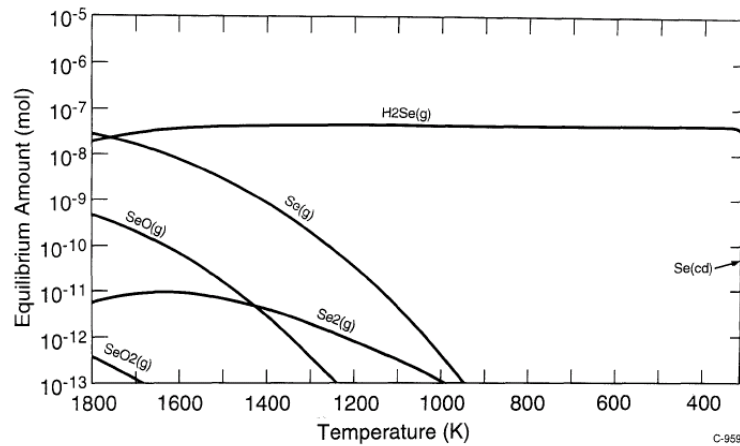


Figure 8: Equilibrium Speciation of Selenium¹⁵

2.2.2 IGCC Projects

There are several IGCC projects that have been completed. The first successful project was located in Southern California at the Cool Water Project between 1984 and 1989. In Florida, the 250 MW Polk Power Station broke ground in 1994. In 1995, the 262 MW Wabash River project was started in Indiana.⁶

In 1994 the Polk Power Station located in Polk County, Florida was started. It is a 250 MW IGCC, owned by Tampa Electric Company. Tampa Electric Company and its partners received a grant from the Department of Energy for the construction of the clean coal technology at Polk Power Station and it seems that they have achieved it. They have reached 99.5% sulfur removal and between 90-95% mercury removal. Particulate matter (PM) has also been reduced to less than 0.004 lb/Mbtu. Their water usage was reduced by 40% by using less cooling water and also the development of the brine concentration unit, which reuses all of the waste water.¹⁶



Figure 9: Polk Power Station ¹⁷

Destec Energy Inc. and PSI Energy Inc. started the Wabash River Station in West Terre Haute, Indiana in 1995. This was also partially funded by the Department of Energy for the Clean Coal Technology program. From the emissions standpoint, Wabash performed very well. The reported sulfur removal was 96.8% and the particulate matter was reported to be minimal. This project also won *Power Magazine's* 1996 Power Plant of the Year award. At that time, it was the longest-running Integrated Gasification Combined Cycle unit in the U.S. ¹⁸



Figure 10: Wabash Power Station ¹⁹

The power stations described above have demonstrated that IGCC plants are more efficient and environmentally-sound than coal-fired power stations. These projects have provided scientists with experimental data that can be used to further explain and predict the characteristics of coal gasification. With this data, studies can be performed to optimize the energy output of the power stations as well as reduce the amount of pollutant emissions, including SO_x, NO_x, and the trace elements from IGCC power plants.

2.3 Trace Element Emissions

The primary trace elements emitted from coal gasification plants include compounds of As, Se, and Hg. Arsenic compounds released from coal gasification plants include As(s), As₂S₃(s), As₂(g), AsS (g), AsO(g), As(g), AsH₃(g), and AsH(g). The main mercuric compounds present are Hg⁰(g), HgH(g), and HgS(g) and the primary compounds of selenium released from coal gasification plants include Se(g), H₂Se(g), HSe(g), and SeS(g), where (s) represents the solid phase and (g) represents the gaseous phase. The emissions of these species pose numerous health risks to both humans and animals.

2.3.1 Mercury

The EPA has set the Maximum Contaminant Level (MCL) of Hg in drinking water at 2 ppb. The three main forms in which Hg exist are elemental (Hg⁰), inorganic compounds such as mercury salts such as HgCl₂, and organic compounds such as methylated mercury (HgCH₃).²⁰ All three types pose serious health risks.

Mercury occurs naturally in the environment, as a result of volcanoes and forest fires, and can volatilize from water, soil, and flora. However, it is also a result of anthropogenic industrial pollution into the air. These man-made sources include

mining, manufacturing processes, mercury cell production, waste incineration, and crematoria, but the main cause of anthropogenic mercury emissions is from coal-fired power plants.^{21,22}

Mercury emissions accumulate in streams and oceans. When the mercury ends up in the water bacteria chemically transforms it into the organic compound methylmercury which accumulates in the fish that live there. As a result, humans become exposed to HgCH₃ when they eat certain kinds of fish.²³ The main source of mercury in humans is this HgCH₃ ingested during fish consumption and exposure can cause blindness, deafness, speech difficulties, and developmental defects.²⁰ When high levels of mercury are present in the bloodstreams of pregnant and nursing women, they risk harming the developing nervous system of the unborn or newborn child.²⁴

The health risks of elemental mercury (Hg⁰) are also numerous. When Hg⁰ is ingested, it does not pose any serious health threats. However, when inhaled, a large portion enters the brain and can cause damage to the central nervous system.²¹ These effects include tremors, mood changes, and slowed sensory and motor nerve function.²⁰ Ingestion of Hg⁰ can also lead to memory loss, chest pains, and increased susceptibility to kidney damage.²⁴

The toxicity of Hg is dependent upon its speciation. According to *Table 2*, the toxicity of mercuric compounds is as follows:

<u>Toxicity</u>	<u>Species</u>
Most Toxic	Methylated Mercury (HgCH ₃)
	Inorganic Mercury Compounds (i.e. HgH and HgS)
Least Toxic	Elemental Mercury (Hg ⁰)

Table 2: Toxicity of Mercuric Species

Table 2 shows that methylated mercury is the most toxic mercuric compound. Therefore, it is very important that mercury is captured from the flue gases of coal gasification plants before it can accumulate in streams and oceans where it will be chemically transformed to the very toxic methylated mercury.

2.3.2 Arsenic

The EPA has set the MCL of arsenic in drinking water at 10 ppb, effective as of January 23, 2006. The EPA estimates that about 5% of community water systems in the United States had to take corrective action to lower the levels of As that were currently in their drinking water. This accounts for about 3,000 community water systems, which provide water for approximately 11 million people.²⁵

Arsenic is produced by both anthropogenic and natural sources. However, there is three times more arsenic produced by humans as that which occurs naturally in the environment (i.e. in rocks, soil, water, air, plants, and animals²⁶). Man-made industrial sources include copper smelting, mining, and coal burning. However, the major man-made source of arsenic is from coal-fired power plants. Therefore, it is becoming increasingly necessary to reduce the arsenic emitted from coal gasification plants.

Emitted water-soluble forms of As eventually make their way into drinking water. If present in levels that exceed the EPA regulatory standard of 10 ppb, As can cause serious health problems, both short- and long-term. Short-term exposure to arsenic can pose some small health risks, but these effects are not likely from U.S. public water supplies that are in compliance with As regulations. Long-term exposure to arsenic over many years can result in cancer of the bladder, lungs, skin, kidneys, nasal passages, liver and prostate.²⁵ Since As is a carcinogen, there is now evidence that some As compounds can lead to lung and skin cancer. The risk of lung cancer

increases dramatically if exposed to high levels of arsenic trioxide (AsO₃). Skin cancer can be caused by exposure to inorganic As compounds present in drinking water and the air.²⁷

The toxicity of arsenic depends on its speciation. *Table 3* illustrates the relative toxicities of some common As compounds.

<u>Toxicity</u>	<u>Species</u>
Most Toxic	Arsine (AsH ₃)
	Inorganic As(III)
	Organic As(III)
	Inorganic As(V)
	Organic As(V)
Least Toxic	Arsonium compounds and elemental arsenic

Table 3: Toxicity of Arsenic Species²⁷

shows that the most toxic compound of arsenic is arsine (AsH₃), which is a colorless and extremely poisonous gas.²⁷ Arsenite (As(III)), is more toxic than As(V), or arsenate, and inorganic compounds are more toxic than their organic counterparts.

2.3.3 Selenium

The EPA has set the MCL of Se in drinking water at 0.05 ppm. The EPA believes that below this level, humans are not at risk to the negative health effects of exposure to Se.²⁸

Like As and Hg, Se is also a naturally occurring substance in the environment as well as a result of anthropogenic sources. For example, it occurs naturally in fertilized agricultural soil. On the other hand, one of the primary man-made sources is Se

released into the air from coal and oil combustion plants.²⁹

Se is an essential nutrient for human health at low levels. However, when exposed to Se levels at high levels even for a short amount of time, it can pose serious health risks. This exposure can result from Se that is inhaled, ingested, or absorbed through the skin. Humans are exposed to Se through food, water, and contact with soil or air that contains high concentrations of Se.²⁹

The short-term health risks of exposure to Se are numerous. Humans can experience hair and fingernail changes, damage to the peripheral nervous system, fatigue, and irritability when exposed to high levels of Se.³⁰ Eye exposure can result in burning and irritation.²⁹ The long-term effects of Se include hair and fingernail loss, kidney damage, liver tissue damage, and damage to the nervous and circulatory systems.²⁸ Se primarily accumulates in the liver and kidneys, where it can cause Se poisoning, also known as selenosis.³⁰ Selenosis can become so severe that it can result in death.²⁹

Table 4 illustrates the relative toxicities of selenium compounds of interest.

<u>Toxicity</u>	<u>Species</u>
Most Toxic	Hydrogen Selenide (H ₂ Se, HSe)
	Selenium Sulfide (SeS)
Least Toxic	Elemental Selenium (Se)

Table 4: Toxicity of Selenium Species³⁰

This table shows that hydrogen selenides, which includes both H₂Se and HSe, are the most toxic selenium compounds of interest. Therefore, emphasis will be placed on these compounds when analyzing the results of subsequent computational chemistry calculations.

Due to the extremely dangerous health effects associated with the compounds of Hg, As, and Se present in the fuel (or syngas) or flue gases of coal-fired power plants, the design of a multi-pollutant sorbent to capture them becomes essential. The number one source of anthropogenic Hg, As, and Se emissions is from coal combustion or gasification plants, and it is very important that their release into the environment is reduced.

2.4 Current Trace Element Removal Practices

There are federal and state regulations that control the emissions from power stations. The control of SO_x and NO_x emissions is very important; the Clean Air Act of 1990 placed a cap on SO_x and NO_x emissions. In a gasifier, the oxygen feed rate is lower than in a pulverized coal system, therefore the sulfur in the gasifier reacts to form H₂S instead of SO_x. In a flue gas desulfurization unit (FGD), better removal efficiency can be achieved when H₂S is the major component (99% removal) compared to SO_x (93% efficiency). The reduction of NO_x emissions can be done with a selective catalytic reduction unit (SCR) and by lowering the flame temperature (low-NO_x burners).⁶

For the trace elements, the pollution control options are not as extensive. For Hg, if it is present in the water-soluble oxidized state (Hg²⁺) it can be partially removed in a wet scrubber.³¹ However, in coal gasification Hg is most likely to be in the elemental state. The technologies used to remove Hg⁰ from gasification applications are molecular sieves and activated carbon.³¹ For arsenic, there have been several attempts to remove the trace element from gasification unit emissions, including molecular sieves (13x), silica gel, alkali metal sorbents, and activated carbon. Arsenic oxide (As₂O₃) is a poison for the vanadium-based SCR catalyst. Therefore, it reduces the amount of NO_x removal when there is no pollution control system in place for As before the SCR unit.³² In the case of Se, the main pollution control technology is

activated carbon. Using a commercially available activated carbon, Lopez-Anton et al. were able to achieve 70% retention for selenium and 20% retention for arsenic in coal gasification simulated syngas at an operating temperature of 120°C.³³

Currently the most promising trace element removal method is activated carbon. However, the gas stream must be cooled to 40-50°C for Hg removal. If metals are used as a sorbent for trace elements, the temperature of the stream can remain between 150-380°C. The following section contains information on the metals that have been considered for potential multi-pollutant sorbents.

2.5 Sorbent Materials

The section justifies our selection of each metal dimer (Au₂, Pd₂, Pt₂, V₂, Fe₂, and Cu₂) for the use in investigating relative binding energies of Hg, As, Se, and H₂S. For each metal, there is a summary of the current uses, supports, and the reason why it may be successful in capturing the species of interest.

2.5.1 Gold

Gold has become particularly interesting in catalysis, because this noble metal, which is unreactive in its bulk form, becomes a highly reactive catalyst when clustered into nanoparticles.³⁴ Gold nanoclusters specifically aid in the oxidation of CO.³⁵ Additionally, these nanoclusters could potentially be useful for adsorbing Hg emissions from coal-fired power plants because historically Hg has been used in mining to capture Au³⁶. Since Au and Hg are commonly found together in nature, Au sorbents may be successful in capturing Hg. This work also seeks to determine if Au could be used to adsorb As and Se as well, and in the future be used as a multi-pollutant sorbent in coal gasification.

Recently, studies of Au nanoclusters have been focused on modeling or experimentally creating the clusters on a support surface, or on the oxidation of CO on the Au cluster. The nanoclusters can behave in different ways depending upon the support material. Additionally, the support material potentially could aid in the catalysis of a reaction in some circumstances. Au nanoclusters typically have oxide supports, which are classified as reducible-oxide supports (TiO_2 , TiO_3 , NiO , Fe_2O_3 , etc.) or irreducible-oxide supports (Al_2O_3 , MgAlO_4). In general, for reasons which are yet to be determined, reducible oxide supports are more stable than irreducible supports.³⁷

This study focuses on understanding the chemistry of Hg, As, and Se with Au dimers to determine if Au should be considered as a multi-pollutant sorbent.

2.5.2 Palladium

Palladium has been used as a catalyst for many applications. The most common use is as a catalyst for hydrogenation reactions including the hydrogenation of alkenes, arenes, olefins, and unsaturated fatty acid esters.³⁸ There are other chemical reactions that utilize the catalytic activity of Pd such as the Suzuki reaction (formation of carbon to carbon single bonds) and carbonylation (the addition of CO to an organic compound to create a carbonyl group).³⁹ Palladium is very reactive, which is why it is frequently used as a catalyst for chemical reactions.

The amount of surface area on a catalyst is directly proportional to the efficiency of the catalyst. The more surface area available on the catalyst the more active sites that are accessible for the reaction to take place on. To increase the surface area of catalytic compounds, nanoparticles are used. The surface areas of various support materials are shown in *Table 5*. In the case of Pd, nanoparticles have been made either

on surfaces of solid supports such as silica and alumina, or colloidal particles.³⁹ A study has successfully made monodisperse Pd nanoparticles using a Pd-based surfactant.⁴⁰ Other methods of making nanoparticles include gas-evaporation, sputtering, co-precipitation, sol-gel, hydrothermal, and microemulsion techniques.⁴¹ Sometimes supports can be used to create a greater amount of surface area for the reaction to occur.

Support	Surface Area (m ² /gram)
Activated Carbon	1100 ⁴²
Silica (SiO ₂)	200 ^{42 above42}
Alumina (Al ₂ O ₃)	90 ⁴²
Au	1-3 ⁴³
Pd	1-3 ⁴³
Pt	45 ⁴³
V	130-150 ⁴³
Fe	30-50 ⁴³
Cu	30-70 ⁴³

Table 5: Surface Area of Support Materials

A support of a catalyst consists of varying geometries and sizes to create a large network of sites for the catalyst to be attached to. The most popular type of support for Pd is activated carbon (Auer 1998). Other types of supports include aluminum (Al), alumina (Al₂O₃), titanium oxide (Ti₂O₃), silica (SiO₂), and zirconia oxide (ZrO₂).^{44,45,46,47,48} The wide range of possible supports creates choices that can help to optimize the activity of the Pd catalyst, which is important especially when the cost of Pd is taken into account.

2.5.3 Platinum

The use of Pt as a catalyst has been a heavily-studied research topic for many years. The two major uses of Pt catalyst are for the cathode material in direct methanol fuel cells (DMFC) and as a catalyst in a three-way catalytic converter (TWC).^{49,50} A TWC converts NO and CO to NO₂ and CO₂ simultaneously. Fuel cells are a main target for future sources of clean energy. Therefore, the increase in efficiency of fuel cells is

crucial to the Pt catalyst development. Understanding the characteristics of and other applications for the Pt catalyst will only help the energy industry.

Pt catalysts have better efficiency as their surface area increases; therefore the use of nanomaterials to support Pt could be very useful. Mizukoshi et al. found that Pt particles could be made from Pt ions (Pt (II)) after sonication with sodium dodecyl sulfate (SDS).⁵¹ Another study concluded that carbon nanotubes could be a possible support for the Pt catalyst.⁵² Additional supports materials investigated include aluminum (Al), activated carbon (C), cesium-zirconia alloys (Ce-Zr), titanium oxide (TiO₂), niobium oxide (Nb₂O₃), yttrium oxide (Y₂O₃), vanadium oxide (V₂O₃), zirconia oxide (ZrO₂), alumina (Al₂O₃), chromium carbide (Cr₃C₂), silicon (Si₃), and nitrogen (N₄).^{53,54,55,56,50} With all of these different supports, Pt catalyst can be made to have a high surface area.

2.5.4 Vanadium

Vanadium oxide is often used as a catalyst with similar properties to Pt.⁵⁷ Additionally, V is used as the active catalyst within Selective Catalytic Reduction (SCR) units to reduce NO_x⁵⁸, so it would be beneficial if V could be used to capture additional pollutants. This research seeks to understand the fundamental chemistry between V and the trace element species. Thus, dimers of V are being considered as a sorbent for trace elements (Hg, As, and Se) from the flue and fuel gases of coal combustion and coal gasification.

Currently V catalysts are used to enhance the reaction: SO₂ → SO₃. This catalyst is operated at temperatures below 650°C, and can be poisoned by various materials including: Hg, (Se), and (As₂O₃). The pentoxide form of arsenic, As₂O₅ has been known to block the catalyst surface around 600°C. The species, Se and SeO₃ only

have been shown to cause harm to the catalyst below 400°C, and initial activity is restored after heating the catalyst. Additionally, Hg has been known to deposit on the catalyst surface further reducing the catalyst activity. Elemental Hg has been known to prevent deposition of SO₂ on the V catalyst surface.⁵⁹ Therefore, V could potentially be used to capture As at high temperatures around 600°C, Se at temperatures below 400°C, and elemental Hg.

2.5.5 Iron

An Fe sorbent is being investigated because of its current applications for removing contaminants from the environment, its low cost, and its widespread abundance.⁶⁰ Fe nanoparticles are being used to separate contaminants from groundwater, soil, and sediments.⁶¹ As Wei-xian Zhang of Lehigh University explains, they help remove contaminants from soil and water because when metallic Fe oxidizes in the presence of contaminants such as trichloroethene, carbon tetrachloride, dioxins, or PBCs, the molecules get caught up in the reactions and are broken down into simple carbon compounds that are less toxic than their original state.⁶⁰ Since the particles are on the nanometer scale, they are able to flow easily through channels in soil and rocks where they can reach and destroy these contaminants.⁶²

Specifically, their ability to remove carbon tetrachloride present in groundwater is being studied. Researchers at the Oregon Graduate Institute School of Science and Engineering have discovered two types of Fe nanoparticles that are able to perform this contaminant removal, which range in size from 10 to 100 nanometers. The first one was an iron oxide with a magnetic shell consisting of mostly sulfur, which was proven to be able to degrade carbon tetrachloride to harmless products. The second was an iron oxide coated in oxidized boron. This attempt was not as successful because although it degraded the carbon tetrachloride, it also produced the

contaminant chloroform.⁶¹

Studies have been conducted to analyze the most effective support for Fe nanoparticles. Supports composed of MgO and CeO₂ have been studied. These investigations show that CeO₂ is the most effective support for these nanoparticles. This is most likely due to the exchange of electrons at the interface between the Fe₂O₃ catalyst and the CeO₂ support. The formation of a methoxy group at the surface also contributes to this increased catalytic activity.⁶³

The relatively low cost of Fe nanoparticles makes it an attractive option for the removal of contaminants. The cost of these nanoparticles is roughly \$40 to \$50 per kilogram. Since approximately 11.2 kilograms of Fe nanoparticles are needed to decontaminate approximately 100 square meters of land, this equates to only about \$5 per square meter.⁶⁰ Consequently, their inexpensive nature and high ability to remove contaminants from the soil and water makes them an attractive option for the removal of the harmful compounds of Hg, Se, and As from coal gasification plants. One drawback to Fe is that it oxidizes quickly, which should be considered when using Fe in oxidizing environments. However, coal gasification takes place in a reducing environment, so this may not be of concern.

2.5.6 Copper

The final sorbent being studied is Cu, an economical catalyst with important properties. Nanoclusters of metallic Cu have been supported on different metal oxide supports, including ZnO, ZrO₂, Al₂O₃, and SiO₂.⁶⁴ These catalysts are used widely in many industrial applications. The greatest catalytic activity is achieved when Cu nanoparticles less than 4 nanometers are supported on metal cerium oxide, or ceria. Chemist Jose Rodriguez, who is currently conducting research at the U.S. Department

of Energy's (DOE) Brookhaven National Laboratory, said that “Metal nanoparticles alone are not able to do the catalysis, but when you put them on the ceria, you see tremendous catalytic activity.”⁶⁵

Research is being conducted for the use of Cu nanoparticles in reactions that improve the life of fuel cells. Currently, Au nanoparticles are being used, but Cu nanoparticles are being investigated as a substitute because they are much cheaper. Research performed by Jose Rodriguez has shown that Cu nanoparticles can replace Au nanoparticles. While Au has proven to demonstrate the greatest catalytic activity, Cu continues to be investigated because it is almost as reactive as Au and it is a lot less expensive.⁶⁵ As a result, these Cu nanoparticles are being investigated for the removal of Hg, Se, and As compounds from coal gasification environments because of their proven catalytic activity for other applications, and most importantly, their inexpensive cost.

2.5.7 Cost Comparison of Sorbent Materials

In addition to the current uses and material properties of each potential metal sorbent, we must also consider the cost of each material when recommending the use of each metal as a sorbent material. Pt, Au, Pd, Fe, V, and Cu are the metals of interest from highest cost to lowest cost⁶⁶ as shown in *Table 6*.

<u>Metal</u>	<u>US Dollars/ kg</u>
Pt	59,857
Au	32,135
Pd	13,545
Fe	194
V ₂ O ₅	18.52
Cu	7.02

Table 6: Cost Comparison of Sorbent Materials

2.6 Computational Chemistry

One aim of computational chemistry is to model chemical reactions and predict molecular properties.⁶⁷ The quantum-chemical program used in this work is Gaussian 03W. It is an *ab initio* solver, which translates to “based upon first principles,” meaning it does not use any empirical relations. Gaussian has the ability to investigate compounds that are in the gas phase, solution phase, solid state, or excited state.⁶⁸

The Gaussian software package allows for the calculation of estimated solutions of the Schrödinger Wave Equation (SWE) to determine the energies of the individual molecules or bound complexes. This equation is solved using a specified mathematical method and basis set combination that must first be defined by the user. All the results are based on solutions of the SWE given the appropriate wavefunction(s). For a single electron, the time independent SWE becomes

$$\hat{H}\Psi = E\Psi \quad (1)$$

where \hat{H} is the Hamiltonian operator, E is the energy eigenvalue, and Ψ is the eigenfunction (i.e., wavefunction). Computational chemistry programs use complex algorithms and iterations to solve approximations to the SWE to find stable optimum values for such parameters as bond lengths, energies, and vibrational frequencies.

The two most important parameters that the user must specify are the method of approximating the wave equation with the basis set. Together, these parameters make up the “level of theory,” which will depend on the system that is being modeled. The full Hamiltonian, and hence, the SWE, can never be completely solved except for a system that consists of a single electron and, different methods allow for different approximations of the Hamiltonian.⁶⁹ These methods include efficient ones such as B3LYP (Becke 3-Parameter, Lee, Yang, and Parr), and more complex methods such

as QCISD (Quadratic Configuration Interaction with Single and Double Excitations) and CCSD (Coupled Cluster with Single and Double Excitations). The amount of time necessary to complete calculations increases as higher and more accurate methods are used for the systems analyzed. Therefore, one needs to establish a balance between efficiency and accuracy when using computational chemistry methods. However, the accuracy of computational chemistry software programs such as Gaussian is increasing to such an extent that it is able to compete with results derived experimentally.⁶⁷

The second parameter is the basis set, which describes the space that the electrons can occupy. Basis sets may also contain polarization and/or diffuse functions, which can greatly affect the calculated parameters. Polarization functions, denoted by one or two asterisks add an additional p-function to the basis set. One asterisk (*) adds polarization functions to all atoms other than hydrogen, while two asterisks (**) provides polarization functions for all atoms in the system. Polarization functions give more flexibility to the basis set by adding d-type functions to basis sets with p-orbitals and f-type functions to basis sets with d-type orbitals.⁷⁰ Diffuse functions, on the other hand, are denoted by plus signs. One plus sign (+) indicates that a diffuse function is added to all atoms other than hydrogen, while two plus signs (++) show that diffuse functions are added to all atoms of interest. Diffuse functions are mainly used to provide more accurate descriptions of anions by improving the basis set at large distances from the nucleus.⁷¹

To speed up calculations for systems with many electrons, we sometimes utilize effective core potentials (ECPs). ECPs neglect the electron correlation between inner and valence electrons. Therefore, only the bonding and behavior of the valence

electrons can be studied.⁷² It is particularly useful for systems with Au and Hg, which have many electrons.

The calculations are sensitive to the method and basis set chosen, which is why careful consideration must be given to these choices. Calculations should be run at selected levels of theory for species of known parameters to see which produces geometries and vibrational frequencies that agree best with experimental data. After a level of theory has been found, further calculations can be made with Gaussian using this justified level to study more complex species.

2.7 Summary

The background information provides an overview of the scope of this MQP within the context of global and national coal consumption, coal gasification, and the harmful effects of the trace element species of interest. Additionally, this section contains the justification for choosing the sorbent materials of interest based on the current catalytic uses and potential for adsorbing the trace element species. Computational chemistry was used to model the binding of the trace element species with the metal dimers. The methodology section describes how these reactions were studied using computational chemistry techniques.

CHAPTER 3: METHODOLOGY

This methodology explains how the binding energies between the trace element species of Hg, As, and Se were computed. When using Gaussian, after the level of theory has been validated, the energetics of the individual species and bound complexes within each reaction being analyzed were determined, and finally the binding energy (BE) was computed. For the reactions with the strongest BEs, the energy differences between the HOMO and LUMO of the reactants are examined and an orbital analysis is conducted. The overall methodology is summarized in *Table 7*, and discussed more thoroughly in Sections 3.1 to 3.6.

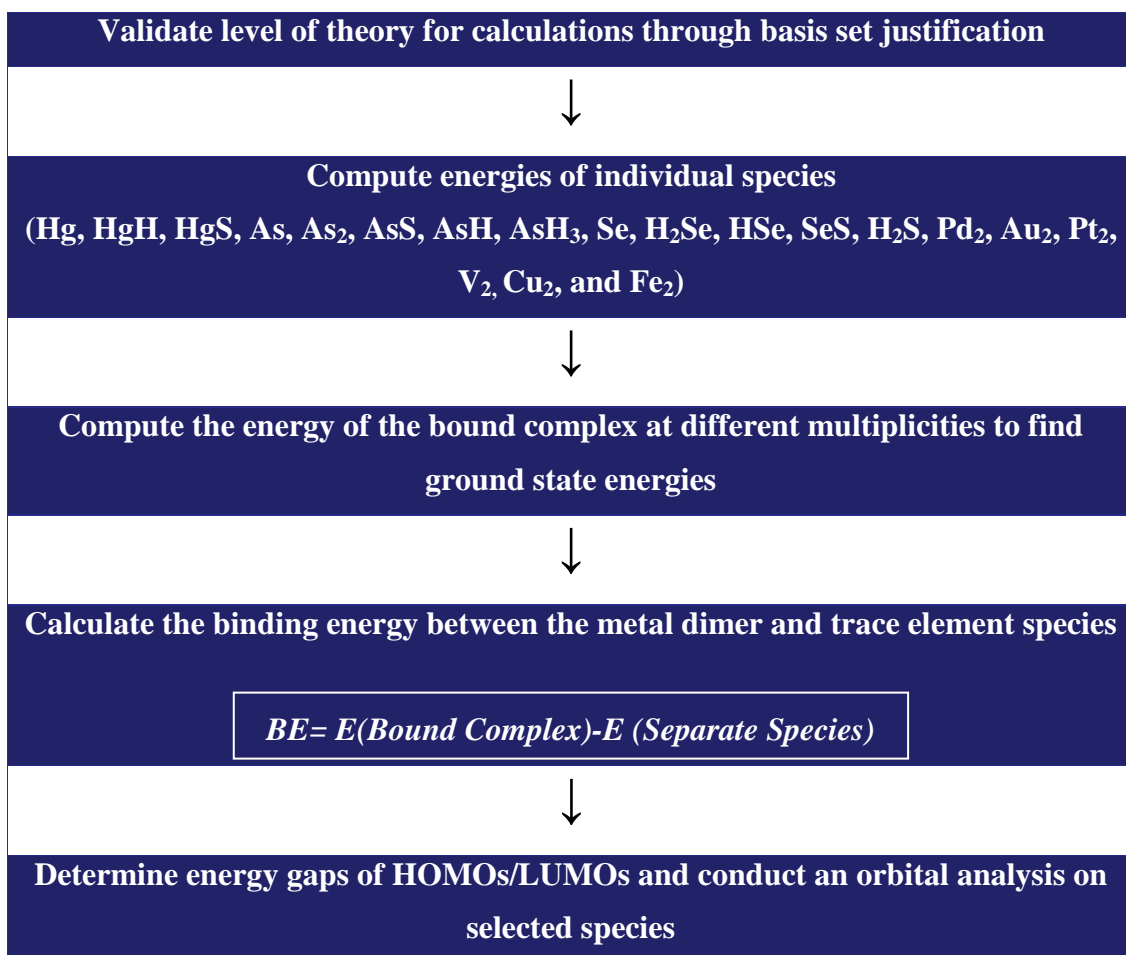


Table 7: Summary of Methodology

3.1 Level of Theory Justification

The methods investigated to approximate the wave equation were B3LYP, a relatively efficient model that relies on Density Functional Theory calculations, and QCISD, which is a more complex calculation that involves the Hartree-Fock approximation and all configurations that are derived from singles and doubles excitations. The configuration simply refers to the arrangement of the electrons. It is an effective method for describing systems in the ground state, such as the ones that we are modeling.⁷³ The basis sets considered for the metal dimers each consisted of a relativistic effective core potential (ECP). They were Stevens/Bauss/Krauss 1992 (SBKJCVZ ECP) and Stuttgart 1997 (ECP60MDF). Additionally, LANL2DZ was considered for Fe calculations. The basis set considered for As and Se was 6-311G* and for Hg was ECP60MDF. Hg has more than double the amount of electrons, and therefore requires a different basis set to achieve an accurate model.

The accuracy of the level of theory for each component of the reaction was determined by comparing the calculated theoretical vibrational frequency predictions and/or bond lengths of each species to the experimental values found within the literature. The validation of the level of theory chosen will be presented in the results and discussion section of this report.

3.2 Ground-State Multiplicities

An important quantity specified in the Gaussian input file is spin multiplicity. The multiplicity represents the total number of orientations of the spin angular momentum corresponding to the total spin quantum number of all electrons (S)⁷⁴ and is defined as $2S+1$. A system with a multiplicity of one has all the electrons paired and is called a single. One unpaired electron would be a doublet, with a multiplicity of two, and so on.

We found the ground state of our species through calculations carried out at different multiplicities. Since the determination of the exact electron configuration of the bound species is a complicated procedure, we calculated the binding energy of each complex for 3 to 4 different multiplicities. The multiplicity of the species yielding the lowest energy was said to be the ground state. The binding energy of the ground state was used as the basis for comparison of all the bound species.

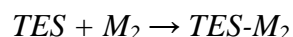
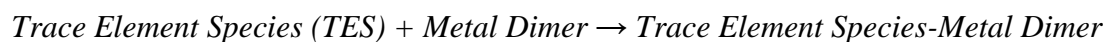
3.3 Orientation of Reactions

In addition to the multiplicity, another important specification in the Gaussian input file was the orientation of the reaction. Certain compounds of Hg, As, and Se may bind to the metal dimer differently, depending on the orientation of the reaction; such compounds include HgS, AsS and SeS. For example, a molecule of HgS could bind to the metal dimer on the Hg side or the S side depending on its preferred orientation. Calculations were carried out in Gaussian that accounted for all possible orientations. As a result, the species that exhibited the strongest binding energy could be said to be the preferred orientation of that particular reaction.

3.4 Binding Energy

To determine the binding energy of the adsorbed species on each of the metal dimers the energy of the individual species alone and the energy of the product were determined initially. To ensure consistency within our binding energy results, we used the same level of theory for all of the calculations, i.e., B3LYP, and the corresponding basis sets for each element were held constant. We also used the multiplicities corresponding to the ground state for all of the binding energy calculations to ensure trends associated with the strongest binding were revealed.

For simplicity, we considered the binding of the trace element species onto the metal dimers as a reaction in the form:



The energy required to complete this reaction is calculated according to 1,

$$\Delta E = \sum E_{\text{Products}} - \sum E_{\text{Reactants}} \quad (1)$$

such that the product is the adsorbed trace element species on the metal dimer and the reactants are the individual compounds. From the Gaussian output, the energy of the molecule is given in Hartrees, which was converted to the more common energy unit, kcal/mol, using a conversion factor of 627.5095 Hartrees per kcal/mol after calculating binding energies in Hartrees.

Additionally, the type of adsorption, i.e., chemisorption or physisorption was determined. If the BE is calculated to be over 15 kcal/mol, an adsorption mechanism associated with chemisorption is most likely occurring. If the BE is calculated to be less than 10-15 kcal/mol an adsorption mechanism associated with physisorption is likely to be occurring. The calculation of the BE of each reaction helps to show the strongest bonds between the metals and trace element specimen, and thus the strongest candidates for a multi-pollutant sorbent.

3.5 HOMO and LUMO Maps

HOMO (Highest Occupied Molecular Orbital) and LUMO (Lowest Unoccupied Molecular Orbital) maps were generated for the metal dimers, trace element species, and bound complexes. The distribution of these orbitals are allows us to further understand the transfer of electron density during the binding of the trace element species on the metal dimers and help to determine the material with the highest potential to be used as a multi-pollutant sorbent.

In Gaussian03, the keyword “formcheck” created a formcheck file that was opened in Gaussview to visualize the molecular orbitals. From the entire list of molecular orbitals, we chose only the HOMO and LUMO maps. However, in the transition metals there are likely to be a greater number of molecular orbitals participating in the interactions, so further work should be done to analyze these higher order contributions. The energy of the HOMO and LUMO orbitals was provided, and can be used to determine which species, the trace element or the metal dimer, was donating the electrons and which one was accepting the electrons during the reaction. We defined two energy differences between the HOMO and LUMO energies, ΔE_{HL} , as follows: $\Delta E_A = (\text{HOMO}_{\text{Reactant 1}} - \text{LUMO}_{\text{Reactant 2}})$ and $\Delta E_B = (\text{HOMO}_{\text{Reactant 2}} - \text{LUMO}_{\text{Reactant 1}})$. The smallest difference represented the more likely exchange of electrons from the HOMO of one species to the LUMO of the other. ΔE_{HL} 's and HOMO/LUMO maps were generated for reactions with particularly strong BEs. Using these HOMO/LUMO images, we will generate orbital diagrams for visualizing the most promising sorbent material.

3.6 Orbital Analysis

Orbital diagrams are a tool will help us visualize how the electrons redistribute themselves following the binding of these species on the metal dimer. For this analysis, we will analyze energy differences to determine the species that is donating electrons. We will also look at the orbitals of the unbounded and bound complexes to determine how the electron distribution changes upon binding. Finally, we examine the energies of the individual species. If the energies and electron distribution of the HOMO of the dimer with the bound species and the HOMO of the dimer are similar, the properties of the metal should remain similar after binding.

3.7 Summary

This methodology section has described the various steps taken to determine the most effective sorbent for the capture of Hg, As, and Se emissions. It has shown how computational chemistry was used to calculate the binding energies of the bound complexes at different multiplicities and orientations in order to find the ground state. Finally, it has introduced the concept of HOMO/LUMO maps and their relationship to orbital analysis.

CHAPTER 4: RESULTS & DISCUSSION

Within this results and discussion chapter, we (a) justify the level of theory used for each element within our calculations by comparing experimental and calculated vibrational frequency and bond length values, (b) characterize and compare the binding energies of each trace element species on each metal dimer into varying types of adsorption, (c) calculate the HOMO/LUMO ΔE_{HL} 's and create HOMO/LUMO energy maps, and (d) conduct an orbital analysis for the most promising metal dimer with the trace element species.

4.1 Level of Theory Justification

Before determining the binding energies of individual species, the level of theory used for calculations in Gaussian03 was found. The level of theory for Hg⁷⁵ was B3LYP/ECP60MDF, the level of theory for As, Se⁷⁶, and S was B3LYP/6-311G*. The level of theory for each of the metal dimers was determined by calculating the vibrational frequencies and bond lengths of each dimer using both B3LYP/SBKJCVZ ECP and B3LYP/ECP60MDF as shown in *Table 8* and *Table 9*, respectively. Because the experimental and calculated values of the vibrational frequencies and bond lengths were similar, the level of theory for each metal investigated other than Fe was B3LYP/SBKJCVZ ECP. The level of theory for Fe was the B3LYP/LANL2DZ as shown in *Table 10*. A summary of the level of theory chosen for each element is found in *Table 11*.

Dimer	Experimental Vib. Freq. (cm ⁻¹)	ECP60MDF Vib. Freq. (cm ⁻¹)	1992Vib. Freq. (cm ⁻¹)
Pd ₂	210 ⁷⁷	259.75	198.09
Au ₂	190.9 ⁷⁸	158.82	164.69
Pt ₂	259 ⁷⁹	174.89	228.45
V ₂	628 ⁸⁰	708.41	687.16
Cu ₂	265 ⁸¹	257.54	244.11

Table 8: Experimental and Calculated Dimer Vibrational Frequencies

Dimer	Exp. Bond Length (Angstroms)	ECP60MDF Bond Length (Angstroms)	SBKJCVDZ ECP Bond Length (Angstroms)
Pd ₂	2.5	2.36	2.54
Au ₂	2.47	2.59	2.57
Pt ₂	2.34	2.56	2.39
V ₂	1.77	1.71	1.75
Cu ₂	2.22	2.25	2.28

Table 9: Experimental and Calculated Dimer Bond Lengths

Fe ₂	Experimental	SBKJCVDZ ECP	LANL2DZ
Vib. Freq. (cm ⁻¹)	218 ⁸²	328.45	228.2
Bond Length (Angstroms)	2.55 ⁸³	2.20	2.55

Table 10: Experimental and Calculated Fe₂ Vibrational Frequencies and Bond Lengths

Element	Level of Theory
Hg	B3LYP/ ECP60MDF
As, Se, S	B3LYP/ 6-311G*
Au, Pd, Pt, V, Cu	B3LYP/ SBKJCVDZ ECP
Fe	B3LYP/ LANL2DZ

Table 11: Level of Theory Chosen for Each Element

4.2 Binding Energies

All reactions analyzed were only considered in the ground state, since this is the most stable state of each reaction. Binding energies were calculated at three multiplicities ($m= 1,3,5$ or $m=2,4,6$) and the strongest energy was considered the ground state energy. The binding energies were used to predict the type of adsorption. Additionally, we analyze the results based on the trends of each species binding to the various metals. From these analyses we are able to identify particular metals as potential multi-pollutant sorbents based on the strongest binding with multiple trace element species.

4.2.1 Characterization of Binding Energies

Chemisorption, or chemical adsorption, is a type of adsorption that involves valence forces. A strong chemical bond is formed between the element species and metal dimer through a significant rearrangement of the electron density. Alternatively, physisorption, or physical adsorption, involves only bonding by weak intermolecular (Van der Waals) forces. There is no significant change in electron density distribution within the molecule or the metal dimer.⁸⁴ For simplicity, the reactions of interest were categorized by physisorption, chemisorption, or strong chemisorption according to the energies in *Table 12*.

Binding Energy Range	Type of Adsorption
0.1 to 15 kcal/mol ⁸⁵	Physisorption
15 to 50 kcal/mol	Chemisorption
Greater than 50 kcal/mol	Strong Chemisorption

Table 12: Types of Adsorption

4.2.2 Ground-State Binding Energies of Trace Element Species on Metal Dimers

From our analysis of the ground state binding energies, Fe is the best sorbent material for the capture of Hg, As, and Se compounds, as shown by the strongest binding

energies in *Figure 11*. Many of the other metals have a strong attraction for only a particular trace element or two. Although the sorbents chosen for this project have been utilized for capture of some chemical species, we found that Fe had the most potential for the use as a multi-pollutant sorbent for coal gasification. Iron seems to be the most versatile sorbent for the capture of all species considered. Almost all binding energies between trace element species and Fe₂ are greater than 50 kcal/mol (*Figure 11*), demonstrating that all these species have a high affinity for Fe.

The trends in binding from highest binding energy to lowest binding energy for each trace element species on each dimer are represented pictorially by *Table 13*, where the green cells highlight the binding of Fe. This table shows that Fe has the highest binding energy for Hg, HgH, HSe, As, AsS, HAs, and As₂ and second highest binding energy for Se and H₂Se when compared to the other metal dimers modeled.

In addition to having a strong affinity to various trace element species, as discussed previously, Fe has a relatively low cost in comparison to the other materials. Thus, the Fe sorbent will be the focus of subsequent analyses throughout this results and discussion section. Although Fe dimers show strong potential as sorbents, this material could potentially behave differently in the bulk. Fe has a high propensity to oxidize which could subsequently interfere with the adsorption process. Alloying could be used to employ the strong multi-sorbent qualities of Fe. One approach may be to alloy Fe with Cu, which is also an excellent sorbent and is inexpensive.

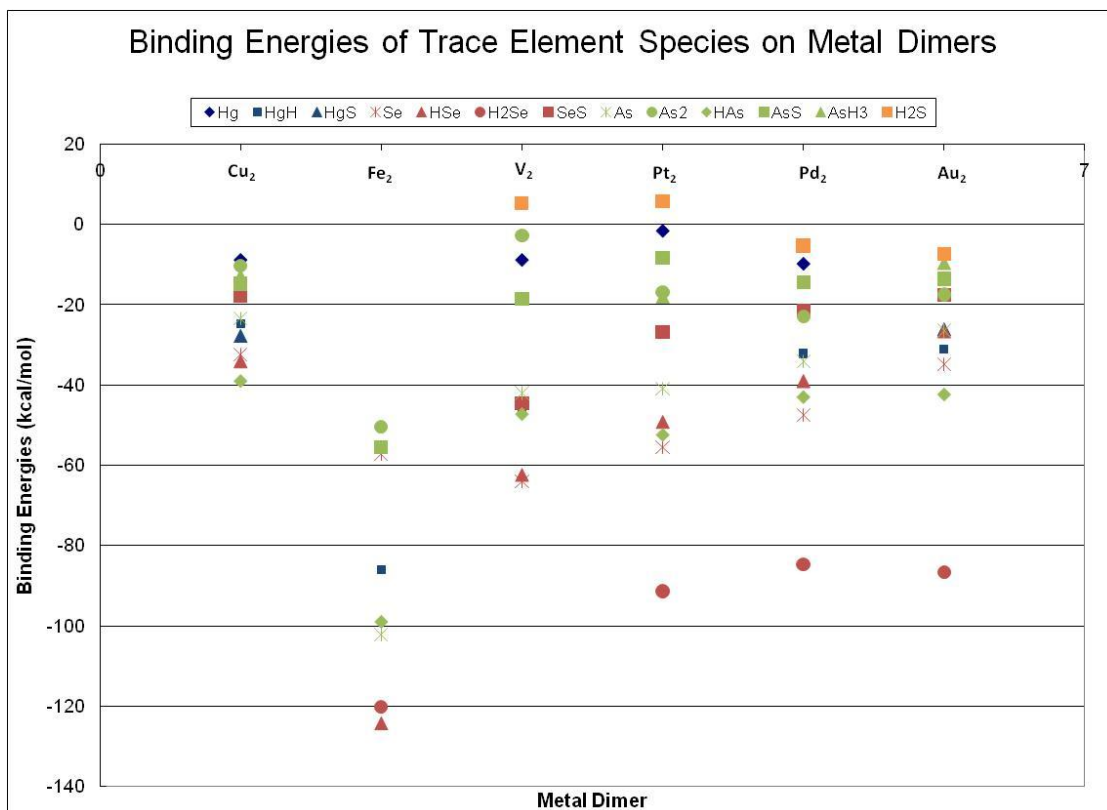


Figure 11: Binding Energies of Trace Element Species on Metal Dimers

Species	Highest BE					Lowest BE
Hg	Fe	Au	Pd	V	Cu	Pt
HgH	Fe	V	Pd	Au	Cu	
HgS	Cu	Au	Pt			
Se	V	Fe	Pt	Pd	Au	Cu
H ₂ Se	Cu	Fe	Pt	Au	Pd	
HSe	Fe	V	Pt	Pd	Cu	Au
SeS	Pt	Pd	Cu	Au		
As	Fe	V	Pt	Pd	Au	Cu
AsS	Fe	Pt	Au	V	Cu	Pd
HAs	Fe	Pt	V	Pd	Au	Cu
AsH ₃	Pt	Cu	Au			
As ₂	Fe	Pd	Au	Pt	Cu	V
H ₂ S	Au	Pd				

Table 13: Fe Binding Energy Trend from Highest BE to Lowest BE

Although Fe demonstrates the strongest binding with the most trace element species of interest, the other five metal dimers also have significant binding energies and

therefore were also considered. Based upon the weak binding energies of trace element species on the Au dimer, Au is the weakest candidate for use as a multi-pollutant sorbent. As shown in *Figure 11*, there is only one Se species with a strong affinity for Au. However, HgS, SeS and AsS have chemisorptions with the Au dimer, which suggests that a stronger sorbent material could potentially be doped or alloyed with Au to adsorb sulfur species.

Palladium also has strong chemisorptions with H₂Se, but has a lower high binding energy for the other species as illustrated in *Figure 11*. Palladium would not necessarily be a bad sorbent, but it does not seem to be the best sorbent for any one type of species.

Figure 11 shows that Pt is an excellent potential sorbent for As and Se species. Nearly all As and Se species have either strong chemisorption or chemisorption with Pt. It may need to be alloyed with another material to create a better sorbent for Hg since it does not bond as well with Pt.

The binding energies for the trace element species on V demonstrate that V could potentially be effective at capturing of these species, though not to the same extent as Pt or Fe. The binding energies shown in *Figure 11* suggest that V has a strong attraction to Hg and Se, but a weaker attraction to As. One option could be to use V alloyed with a material that had a higher binding energy with As, such as Fe.

Calculations show that Cu could be an effective sorbent for the capture of Hg, As, and Se compounds. However, compared to the higher binding energies calculated for the other metal dimers, the attraction of these species to Cu is not as strong. Like V, Cu also shows a stronger attraction to Hg and Se species than it does to As ones. These

trends can be seen in *Figure 11*. Strong chemical bonds exist between Cu and Hg and Se species, whereas weaker Van der Waals forces bind the majority of the As species to Cu.

Our analysis of each individual metal dimer has shown that Au, Pd, Pt, V, and Cu each demonstrate a strong attraction to specific trace element species. However, Fe is the best sorbent for all Hg, As, and Se species as demonstrated by the strong chemisorptions between Fe₂ and nearly all trace element species. In the next section, we analyze the HOMO/LUMO ΔE_{HL} 's and HOMO/LUMO maps of Fe₂ for the trace element species with the strongest binding to Fe₂/the most prevalent species found in coal gasification environments.

4.3 Orbital Analysis of Fe₂

In this section, an orbital analysis is performed for reactions of Fe₂ with Hg, H₂Se, As, and As₂ to determine the movement of electrons during binding. The difference in energy of the HOMO and LUMO (ΔE_{HL}) are also discussed in terms of the binding of Fe₂ with these selected species. The ΔE_{HL} 's between the HOMO and LUMO of the reactants reveal which species is the electron donor. The smaller ΔE_{HL} determines bonding that takes place in the reaction. It is important to note that when the HOMO/LUMO ΔE_{HL} 's are close to one another, this analysis becomes more complicated because interactions other than those between the HOMO and LUMO orbitals may be occurring. This aspect is presented in more detail in the sources of error section of this report.

The orbital analysis allows us to understand how the electrons redistribute themselves following the binding of these species with the metal dimer. If the HOMO of the Fe dimer with the bound species and the HOMO of the Fe dimer are similar, the

properties of Fe₂ probably remain similar after binding. If this is true for the bulk as well, then its stability will make it an attractive option for a multi-pollutant sorbent.

4.3.1 Fe₂ + Hg

Hg is one of the most prevalent species in coal gasification systems and when it binds to Fe₂, the product has a strong binding energy of -44.8315 kcal/mol, representing chemisorption. Due to this strong binding energy and the prevalence of Hg in flue gases, we have calculated the ΔE_{HL} 's between the HOMO and LUMO of the reacting species. All ΔE_{HL} calculations can be viewed in *Tables 20-23* in the Appendix, with the boxed cell representing the smallest energy difference.

The ΔE_{HL} between the HOMO of Fe₂ and LUMO of Hg is the smallest (0.027eV), compared to the ΔE_{HL} between the HOMO of Hg and the LUMO of Fe₂ (-0.126eV). Thus, electrons are donated from the HOMO of Fe₂ to the LUMO of Hg during the formation of HgFe₂. In the HOMO of HgFe₂, the orbitals are mainly around the Fe₂ dimer, as shown in *Figure 12*. This figure also shows that the bond length between the Fe atoms decreases from 2.5477Å to 2.3546Å upon binding of the Hg species, indicating a stronger bond between the Fe₂ dimer upon binding of Hg.

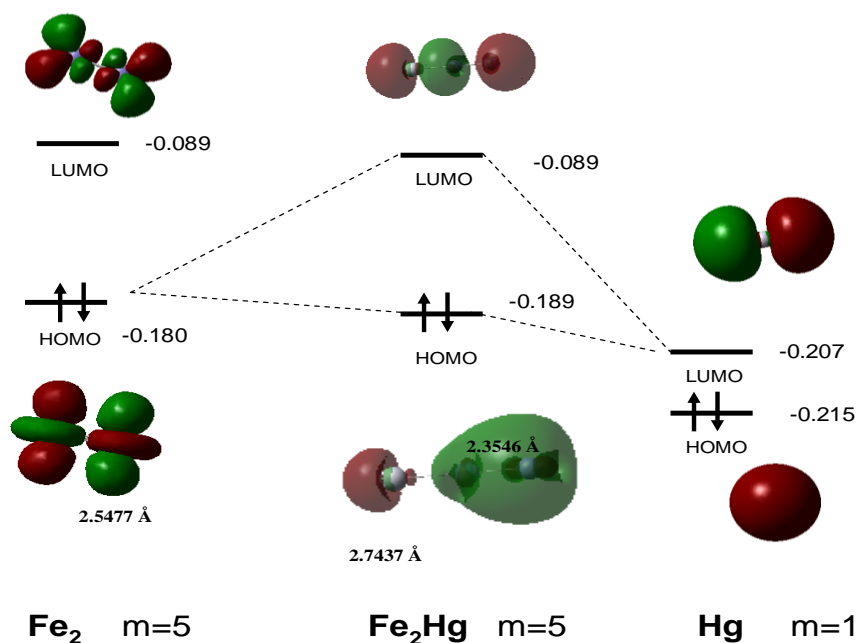


Figure 12: Orbital Analysis of $\text{Fe}_2 + \text{Hg} \rightarrow \text{Fe}_2\text{Hg}$

4.3.2 $\text{Fe}_2 + \text{H}_2\text{Se}$

Of all the trace element species analyzed, H_2Se shows the strongest binding to Fe (-120.257 kcal/mol). In addition, it is also the most prevalent Se species present in coal gasification environments. As a result, H_2Se has been chosen for further analysis.

Since the ΔE_{HL} between the Fe_2 HOMO (-0.180eV) and the H_2Se LUMO (-0.146eV) is smaller than the ΔE_{HL} between the Fe_2 LUMO (-0.089eV) and the H_2Se HOMO (-0.246eV), the Fe_2 HOMO and H_2Se LUMO are the orbitals that interact the most and the Fe_2 donates electrons during the formation of H_2SeFe_2 . This very small ΔE_{HL} of -0.034eV also agrees with the high binding energy of -120.247 kcal/mol of this species.

The HOMO of H_2SeFe_2 depicted in *Figure 13* shows that the orbitals are mainly around the Fe_2 dimer. The HOMO of Fe_2 and the HOMO of H_2SeFe_2 are also close in energy, so the orbitals in H_2SeFe_2 retain some of the structure of Fe_2 . The electrons

will redistribute themselves in the Fe atom not participating in the bonding following binding. Therefore, because the probability of occupancy is higher in the Fe dimer, the dimer will be much more reactive. On the other hand, Se and H₂ are not going to be as reactive.

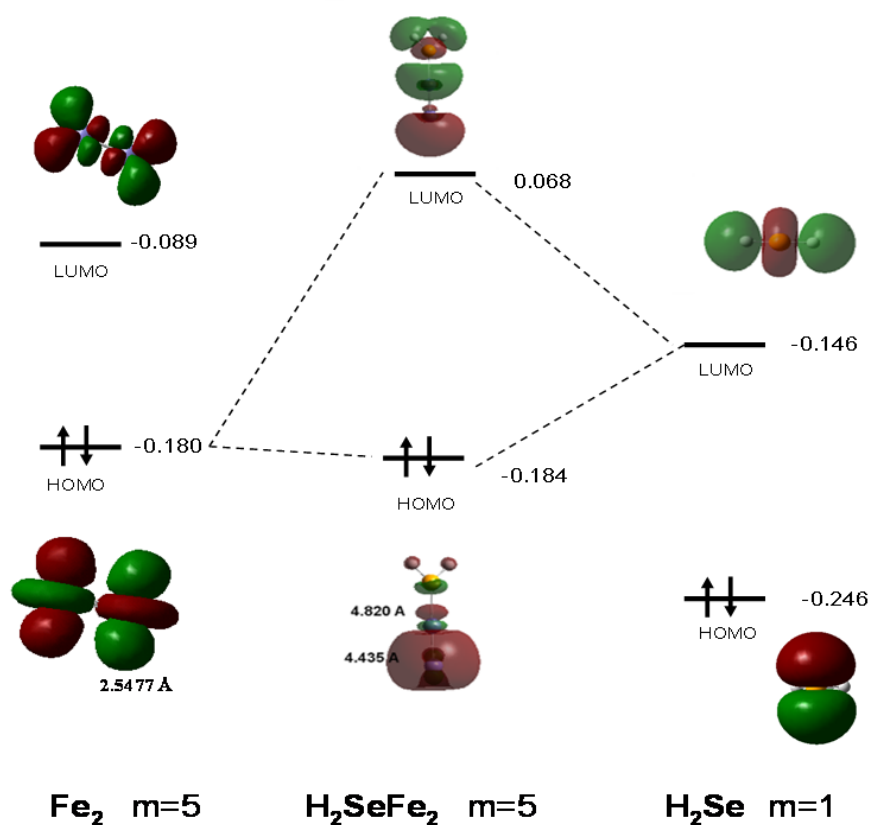


Figure 13: Orbital Analysis of $\text{Fe}_2 + \text{H}_2\text{Se} \rightarrow \text{H}_2\text{SeFe}_2$

4.3.3 Fe₂ + As

The reaction of Fe₂ and As was analyzed because it exhibited one of the highest binding energies of all trace element species at -102.269 kcal/mol. The magnitude of this binding energy suggests strong chemisorption between Fe₂ and As.

The ΔE_{HL} between the HOMO of Fe₂ (-0.180 eV) and the LUMO of As (-0.229 eV) is smaller than that between the HOMO of As and the LUMO of Fe₂. This suggests that the Fe dimer is donating its electrons to As.

Figure 14 shows that the HOMO of AsFe_2 retains some of the original structure of the HOMO of Fe_2 . And as further clarified in the figure, the HOMO of As and the HOMO of AsFe_2 have similar energies to one another. Also, the HOMO of AsFe_2 depicts orbitals around the Fe atoms. Following the binding of As, the electrons will redistribute themselves around the Fe dimer. Therefore, it is also likely that following the binding of As, the AsFe_2 species will be able to bind with the LUMO of another species to form a larger molecule and capture multiple species. This also means that the Fe dimer will be much more reactive than As.

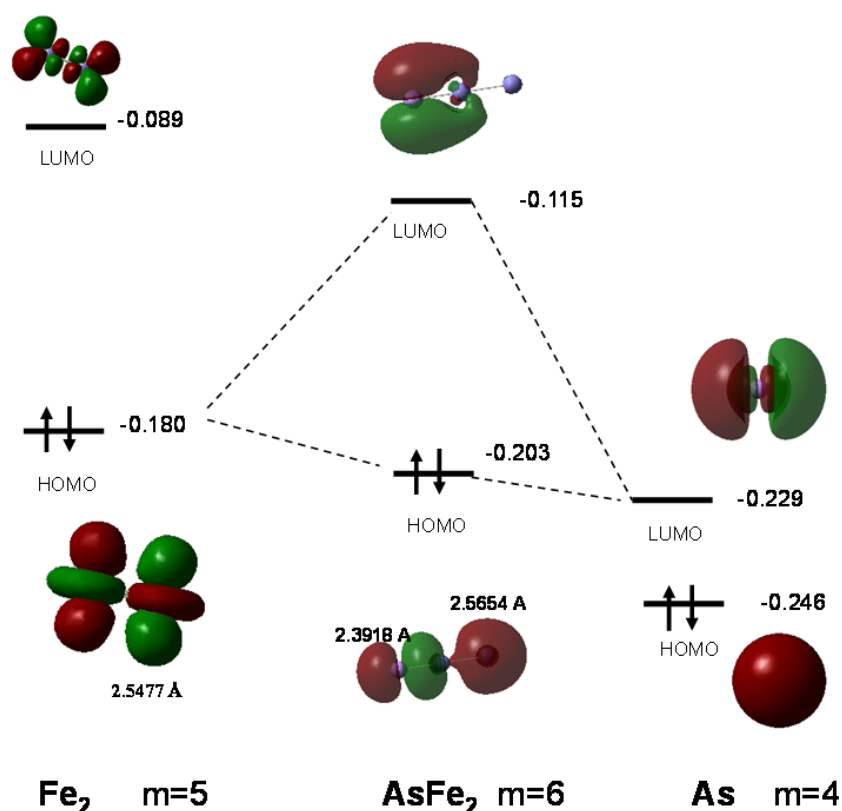


Figure 14: Orbital Analysis of $\text{Fe}_2 + \text{As} \rightarrow \text{Fe}_2\text{As}$

4.3.4 Fe₂ + As₂

The Fe₂ and As₂ reaction was chosen for analysis because As₂ exhibited strong chemisorption with Fe₂. In addition, it is one of the most prevalent As species present in coal gasification environments.

As shown in *Figure 15*, the Fe dimer is most likely donating the electrons to As₂, as demonstrated by the very small ΔE_{HL} of -0.065eV between the HOMO of Fe₂ (-0.180eV) and the LUMO of As₂ (-0.115eV).

The HOMO of As₂Fe₂ gives insight about the redistribution of electrons that occurs following binding. The bond distance of the Fe dimer has decreased from 2.5477Å to 2.3411Å upon absorption of the As₂ molecule while the bond distance of the As₂ species has increased from 2.1116Å to 2.1222Å. This phenomenon also suggests that the Fe molecule has donated its electrons to As because Fe is contracting so the orbitals are getting smaller.

The LUMO of As₂Fe₂ (-0.115eV) and the LUMO of As₂ (-0.115eV) have the same exact energy. Therefore, the LUMO of the bound species retains most of the original electron distribution that is present in the LUMO of the As reactant.

The HOMO and LUMO of the bound complex suggest that As₂Fe₂ may be able to bind to another molecule following the absorption of the As₂ species on the Fe₂ dimer. This may occur because there is significant electron distribution surrounding the HOMO of the Fe atoms of the bound species. Therefore, it is highly likely that the HOMO of As₂Fe₂ will react with the LUMO of another molecule, possibly As₂, to further enhance the absorption of the trace element species of interest on Fe.

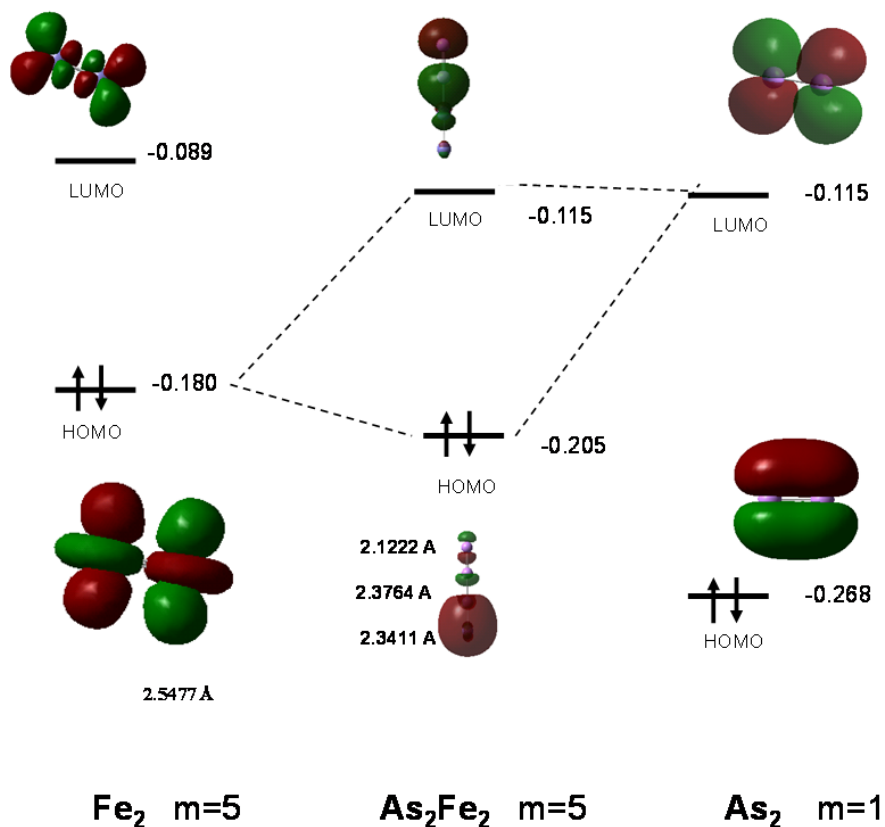


Figure 15: Orbital Analysis of $\text{Fe}_2 + \text{As}_2 \rightarrow \text{Fe}_2\text{As}_2$

4.3.5 Summary of the Orbital Analysis

Our orbital analysis has shown how Fe_2 donates its electrons to the trace element species Hg, H_2Se , As, and As_2 . In addition, following the binding of these species on Fe_2 , the electrons redistribute themselves around the Fe atoms, which is consistent with the strong chemisorption energies associated with the complexes. The HOMO of the bounded complex retains some of the original structure of the Fe dimer. This redistribution of electrons, combined with the small HOMO/LUMO energy of the product, indicate that future reactions are likely to take place between Fe_2 and other trace element species present in the flue gas, so Fe may be able to capture multiple species.

4.4 Sources of Error

There were several sources of error that we encountered in our MQP. First, we only analyzed metal dimers for simplicity. However, we need to take into account the fact that the dimers may behave differently in the bulk. For this reason, we have only analyzed the observed trends. Future research will determine if these dimers follow the same trends in the bulk.

Also, although we have only carried out an in-depth analysis of Fe due to its high binding energies with the trace element species of interest, other metal dimers (Au, Pt, Pd, V, or Cu) may also be effective sorbents for either coal combustion or gasification processes. Some of these dimers demonstrated high binding energies with some of the trace element species, but we did not perform the orbital analysis for these other metal dimers since Fe showed the most potential as a multi-pollutant sorbent. However, we should not neglect the potential capabilities of the other dimers in future analyses.

In the case of the Fe₂ plus Hg reaction, its output file contained (?A) or (?B) notations for the orbital types, which means that Gaussian was not able to resolve the bond type of some of the orbitals during the calculations.

Finally, our analysis has focused solely on the HOMO/LUMO interactions of the metal dimer and trace element species. However, species with smaller HOMO/LUMO ΔE_{HL} 's will have interactions with other orbitals that are similar in energy to the HOMO/LUMO ones. We have not accounted for these additional interactions in this preliminary analysis. Though our efforts in this MQP have tried to minimize all possible sources of error, these are several that have been encountered.

4.5 Summary of Results and Discussion

The goal of our research is to determine a metal to be used as a potential multi-pollutant sorbent. Calculations were carried out using the Gaussian software package employing the levels of theory which best predicted the behavior of each element based on the comparison of calculated values to experimental values. From the binding energy calculations, we determined Fe to be the best sorbent material for species of Hg, As and Se, because nearly all Fe binding energies exhibited a strong chemisorption mechanism, having binding energies over 50 kcal/mol. These results are economically-favorable because the cost of Fe is relatively low when compared to the other sorbent materials considered. To more fully understand the chemistry of the binding interactions, the HOMO/LUMO ΔE_{HL} 's and maps were generated for Hg, H₂Se, As, and As₂, the trace element species most prevalent in coal gasification, and the trace element species with the strongest binding energies.

Our analysis has shown that Fe₂ donates its electrons to the trace element species, but retains some of the original structure of the Fe dimer upon binding. In addition, following the binding of these species on Fe₂, there remains significant electron distribution around the Fe₂ atoms. This electron distribution indicates that reactions will continue to be favorable between Fe₂ and other trace element species present in the flue gas. As a result, each Fe dimer may be able to capture multiple species because the remaining electron density may be able to interact with other pollutants to capture them.

CHAPTER 5: CONCLUSIONS

The search for a multi-pollutant sorbent to be used in coal gasification was the major goal of this MQP. First, the best level of theory was found for the species being studied. This was completed by running several different levels at varying multiplicities to find the ground state and then comparing them to experimental values. The levels of theory used in this project are B3LYP/ECP60MDF for Hg, B3LYP/6-311G* for As, Se, and S, B3LYP/SBKJCVZ ECP for Au, Pd, Pt, V, Cu, and B3LYP/LANL2DZ for Fe.

Using these levels of theory, the binding energies were calculated for the trace element species found in the flue gas of coal gasification plants on each of the metal dimers. It was found that the Fe dimer was the best sorbent for the species studied. The binding energies of Fe with almost all of the trace element species of interest were above 50 kcal/mol, which implies a strong chemisorption mechanism is present. Therefore, it was observed that they all have a strong attraction to Fe.

The binding energies alone do not provide information about the fundamental chemistry that is occurring in these reactions. In order to understand this chemistry, the HOMO/LUMO maps and ΔE_{HL} 's were examined for the binding of Hg, H₂Se, As, and As₂ on the Fe dimer. These trace element species were chosen because they are the most abundant in the coal gasification flue gas. From the HOMO/LUMO maps and ΔE_{HL} 's it was concluded that the Fe atoms donate their electrons to the trace element species during binding.

The ability of Fe to adsorb several types of trace element species found in coal gasification flue gas and its possibility to adsorb these species simultaneously makes it an attractive option for their capture. Its low cost also makes it very practical. Therefore, it has been concluded that Fe has the possibility of acting as a multi-pollutant sorbent to be used in coal gasification at minimal cost.

CHAPTER 6: RECOMMENDATIONS AND FUTURE RESEARCH

From the results and conclusions found in this MQP, it is suggested that further, more in-depth studies be completed for the use of Fe as a multi-pollutant sorbent in coal gasification. Using Gaussian software limits these calculations to dimers, clusters, and nanoparticles. The characteristics of the Fe sorbent in the bulk should be studied to get a more accurate prediction of what will happen when the sorbent is used in experimental studies. Using a different software program such as VASP to study the bulk periodic surface chemical properties would be a very good continuation of this work.

It would also be beneficial to examine how alloying the Fe sorbent with other sorbent materials affects the overall reactivity of the multi-pollutant sorbent. It has already been mentioned that Fe wasn't necessarily the best choice for the capture of some of the trace element species. However, perhaps the Fe sorbent could be alloyed with Au in order to capture the sulfur species. This would also eliminate the possibility of sulfur poisoning the sorbent. Additionally, the impact of the support material for each of the metals will need to be evaluated. The support material could allow the electrons to be concentrated within the support material or within the metal, which could alter the behavior of the sorbent.

The next step in developing this sorbent for the capture of these trace element species in coal gasification processes would be to manufacture the sorbent. The optimal process would be low cost and consistent. Once the sorbent can be manufactured, experimental studies should be done to verify the trends that we have predicted in this

project. In addition, during these experiments the affect of potential poisoning species can be tested. For example, sulfur is known to poison Pd and Pt catalysts and chlorine gas has been shown to affect the reactivity of Fe catalysts.^{86,87} With all of this information, a multi-pollutant sorbent for trace element capture in coal gasification can be designed.

APPENDIX

Reaction	Multiplicity	Ground State BE (kcal/mol)	Adsorption Type
$\text{HgH} + \text{Fe}_2 \rightarrow \text{Fe}_2\text{HgH}$	2	-85.928	Strong Chemisorption
$\text{Se} + \text{Fe}_2 \rightarrow \text{Fe}_2\text{Se}$	1	-57.2783	Strong Chemisorption
$\text{H}_2\text{Se} + \text{Fe}_2 \rightarrow \text{H}_2\text{SeFe}_2$	5	-120.257	Strong Chemisorption
$\text{HSe} + \text{Fe}_2 \rightarrow \text{HSeFe}_2$	8	-124.208	Strong Chemisorption
$\text{As} + \text{Fe}_2 \rightarrow \text{Fe}_2\text{As}$	6	-102.269	Strong Chemisorption
$\text{AsS} + \text{Fe}_2 \rightarrow \text{Fe}_2\text{AsS}$	4	-55.3777	Strong Chemisorption
$\text{HAs} + \text{Fe}_2 \rightarrow \text{HAsFe}_2$	5	-99.0632	Strong Chemisorption
$\text{As}_2 + \text{Fe}_2 \rightarrow \text{As}_2\text{Fe}_2$	5	-50.3182	Strong Chemisorption
$\text{Hg} + \text{Fe}_2 \rightarrow \text{Fe}_2\text{Hg}$	5	-44.8315	Chemisorption

Table 14: Multiplicities and Binding Energies of Fe₂ Reactions

Reaction	Multiplicity (2S+1)	Binding Energy (kcal/mol)	Adsorption Type
$\text{H}_2\text{Se} + \text{Au}_2 \rightarrow \text{H}_2\text{SeAu}_2$	1	-86.7625	Strong Chemisorption
$\text{HgH} + \text{Au}_2 \rightarrow \text{Au}_2\text{HgH}$	2	-31.2090	Chemisorption
$\text{HgS} + \text{Au}_2 \rightarrow \text{Au}_2\text{HgS}$	3	-26.1262	Chemisorption
$\text{Se} + \text{Au}_2 \rightarrow \text{SeAu}_2$	3	-34.8840	Chemisorption
$\text{HSe} + \text{Au}_2 \rightarrow \text{HSeAu}_2$	2	-26.5988	Chemisorption
$\text{SeS} + \text{Au}_2 \rightarrow \text{SeSAu}_2$	3	-17.6597	Chemisorption
$\text{As} + \text{Au}_2 \rightarrow \text{AsAu}_2$	4	-26.4165	Chemisorption
$\text{AsS} + \text{Au}_2 \rightarrow \text{Au}_2\text{AsS}$	2	-23.3648	Chemisorption
$\text{HAs} + \text{Au}_2 \rightarrow \text{HAsAu}_2$	3	-42.4653	Chemisorption
$\text{As}_2 + \text{Au}_2 \rightarrow \text{As}_2\text{Au}_2$	1	-17.5051	Chemisorption
$\text{Hg} + \text{Au}_2 \rightarrow \text{HgAu}_2$	1	-13.6500	Physisorption
$\text{AsS} + \text{Au}_2 \rightarrow \text{AsSAu}_2$	2	-13.5312	Physisorption
$\text{AsH}_3 + \text{Au}_2 \rightarrow \text{Au}_2\text{AsH}_3$	1	-9.6064	Physisorption
$\text{H}_2\text{S} + \text{Au}_2 \rightarrow \text{H}_2\text{SAu}_2$	1	-7.3828	Physisorption

Table 15: Multiplicities and Binding Energies of Au₂ Reactions

Reaction	Multiplicity (2S+1)	Binding Energy (kcal/mol)	Adsorption Type
$\text{H}_2\text{Se} + \text{Pd}_2 \rightarrow \text{H}_2\text{SePd}_2$	3	-84.8421	Strong Chemisorption
$\text{HgH} + \text{Pd}_2 \rightarrow \text{Pd}_2\text{HgH}$	2	-32.3109	Chemisorption
$\text{HgH} + \text{Pd}_2 \rightarrow \text{HgHPd}_2$	2	-34.7761	Chemisorption
$\text{Se} + \text{Pd}_2 \rightarrow \text{SePd}_2$	3	-47.5223	Chemisorption
$\text{HSe} + \text{Pd}_2 \rightarrow \text{HSePd}_2$	2	-38.9784	Chemisorption
$\text{SeS} + \text{Pd}_2 \rightarrow \text{SeSPd}_2$	5	-21.4777	Chemisorption
$\text{SeS} + \text{Pd}_2 \rightarrow \text{SSePd}_2$	5	-17.8373	Chemisorption
$\text{As} + \text{Pd}_2 \rightarrow \text{AsPd}_2$	4	-34.1307	Chemisorption
$\text{HAs} + \text{Pd}_2 \rightarrow \text{HAsPd}_2$	5	-43.1121	Chemisorption
$\text{As}_2 + \text{Pd}_2 \rightarrow \text{As}_2\text{Pd}_2$	1	-22.93	Chemisorption
$\text{Hg} + \text{Pd}_2 \rightarrow \text{HgPd}_2$	3	-9.8237	Physisorption
$\text{AsS} + \text{Pd}_2 \rightarrow \text{AsSPd}_2$	2	-14.4454	Physisorption
$\text{AsS} + \text{Pd}_2 \rightarrow \text{Pd}_2\text{AsS}$	4	-13.8091	Physisorption
$\text{H}_2\text{S} + \text{Pd}_2 \rightarrow \text{H}_2\text{SPd}_2$	3	-5.3560	Physisorption

Table 16: Multiplicities and Binding Energies of Pd₂ Reactions

Reaction	Multiplicity (2S+1)	Binding Energy (kcal/mol)	Adsorption Type
$\text{Se} + \text{Pt}_2 \rightarrow \text{SePt}_2$	3	-55.4743	Strong Chemisorption
$\text{H}_2\text{Se} + \text{Pt}_2 \rightarrow \text{H}_2\text{SePt}_2$	3	-91.4993	Strong Chemisorption
$\text{HAs} + \text{Pt}_2 \rightarrow \text{HAsPt}_2$	1	-52.5308	Strong Chemisorption
$\text{HSe} + \text{Pt}_2 \rightarrow \text{HSePt}_2$	4	-49.1751	Chemisorption
$\text{SeS} + \text{Pt}_2 \rightarrow \text{SeSPt}_2$	1	-25.8594	Chemisorption
$\text{SeS} + \text{Pt}_2 \rightarrow \text{SSePt}_2$	1	-26.9127	Chemisorption
$\text{As} + \text{Pt}_2 \rightarrow \text{AsPt}_2$	4	-40.957	Chemisorption
$\text{AsS} + \text{Pt}_2 \rightarrow \text{Pt}_2\text{AsS}$	2	-48.0152	Chemisorption
$\text{AsH}_3 + \text{Pt}_2 \rightarrow \text{Pt}_2\text{AsH}_3$	1	-18.0468	Chemisorption
$\text{As}_2 + \text{Pt}_2 \rightarrow \text{As}_2\text{Pt}_2$	1	-16.8215	Chemisorption
$\text{Hg} + \text{Pt}_2 \rightarrow \text{HgPt}_2$	1	-1.6470	Physisorption
$\text{AsS} + \text{Pt}_2 \rightarrow \text{AsSPt}_2$	6	-8.3505	Physisorption
$\text{H}_2\text{S} + \text{Pt}_2 \rightarrow \text{H}_2\text{SPt}_2$	1	5.5972	Endothermic Rxn.

Table 17: Multiplicities and Binding Energies of Pt₂ Reactions

Reaction	Multiplicity	Ground State BE (kcal/mol)	Adsorption Type
$\text{Se} + \text{V}_2 \rightarrow \text{V}_2\text{Se}$	3	-64.0454	Strong Chemisorption
$\text{HSe} + \text{V}_2 \rightarrow \text{HSeV}_2$	6	-62.3588	Strong Chemisorption
$\text{HgH} + \text{V}_2 \rightarrow \text{V}_2\text{HgH}$	4	-46.6038	Chemisorption
$\text{SeS} + \text{V}_2 \rightarrow \text{SeSV}_2$	1	-44.6136	Chemisorption
$\text{As} + \text{V}_2 \rightarrow \text{V}_2\text{As}$	6	-42.0234	Chemisorption
$\text{AsS} + \text{V}_2 \rightarrow \text{V}_2\text{AsS}$	6	-18.4365	Chemisorption
$\text{HAs} + \text{V}_2 \rightarrow \text{HAsV}_2$	5	-47.3622	Chemisorption
$\text{As}_2 + \text{V}_2 \rightarrow \text{V}_2\text{As}_2$	5	-2.8324	Physisorption
$\text{V}_2 \rightarrow \text{V}_2\text{Hg}$	3	-8.870	Physisorption
$\text{H}_2\text{S} + \text{V}_2 \rightarrow \text{H}_2\text{SV}_2$	5	5.1003	Endothermic Reaction

Table 18: Multiplicities and Binding Energies of V_2 Reactions

Reaction	Multiplicity	Ground State BE (kcal/mol)	Adsorption Type
$\text{H}_2\text{Se} + \text{Cu}_2 \rightarrow \text{H}_2\text{SeCu}_2$	1	-712.13	Strong Chemisorption
$\text{HgH} + \text{Cu}_2 \rightarrow \text{Cu}_2\text{HgH}$	2	-24.935	Chemisorption
$\text{HgS} + \text{Cu}_2 \rightarrow \text{HgSCu}_2$	3	-27.7846	Chemisorption
$\text{Se} + \text{Cu}_2 \rightarrow \text{Cu}_2\text{Se}$	3	-32.4534	Chemisorption
$\text{HSe} + \text{Cu}_2 \rightarrow \text{HSeCu}_2$	2	-34.0739	Chemisorption
$\text{SeS} + \text{Cu}_2 \rightarrow \text{Cu}_2\text{SeS}$	3	-17.7803	Chemisorption
$\text{As} + \text{Cu}_2 \rightarrow \text{Cu}_2\text{As}$	4	-23.4438	Chemisorption
$\text{HAs} + \text{Cu}_2 \rightarrow \text{HAsCu}_2$	3	-39.1365	Chemisorption
$\text{Hg} + \text{Cu}_2 \rightarrow \text{Cu}_2\text{Hg}$	1	-8.8660	Physisorption
$\text{AsS} + \text{Cu}_2 \rightarrow \text{AsSCu}_2$	2	-14.7697	Physisorption
$\text{AsH}_3 + \text{Cu}_2 \rightarrow \text{Cu}_2\text{AsH}_3$	1	-12.8398	Physisorption
$\text{As}_2 + \text{Cu}_2 \rightarrow \text{Cu}_2\text{As}_2$	1	-10.3703	Physisorption

Table 19: Multiplicities and Binding Energies of Cu_2 Reactions

$\text{Fe}_2 + \text{Hg} \rightarrow \text{Fe}_2\text{Hg}$		ΔE_{HL}	
	Fe_2	Hg	
HOMO	-0.18	-0.215	0.027
LUMO	-0.089	-0.207	

Table 20: HOMO/ LUMO ΔE_{HL} 's of $\text{Fe}_2 + \text{Hg} \rightarrow \text{Fe}_2\text{Hg}$

Fe₂+H₂Se → H₂SeFe₂			ΔE_{HL}	
	Fe ₂	H ₂ Se	Fe ₂ to H ₂ Se	H ₂ Se to Fe ₂
HOMO	-0.18	-0.246	-0.034	-0.157
LUMO	-0.089	-0.146		

Table 21: HOMO/ LUMO ΔE_{HL}'s of Fe₂ + H₂Se →H₂SeFe₂

Fe₂+As→Fe₂As			ΔE_{HL}	
	Fe ₂	As	Fe ₂ to As	As to Fe ₂
HOMO	-0.18	-0.246	-0.049	-0.157
LUMO	-0.089	-0.229		

Table 22: HOMO/ LUMO ΔE_{HL}'s of Fe₂ + As →Fe₂As

Fe₂+As₂→Fe₂As₂			ΔE_{HL}	
	Fe ₂	As ₂	Fe ₂ to As ₂	As ₂ to Fe ₂
HOMO	-0.180	-0.268	-0.065	-0.179
LUMO	-0.089	-0.115		

Table 23: HOMO/ LUMO ΔEHL' s of Fe₂ + As₂ →Fe₂ As₂

BIBLIOGRAPHY

- ¹ Energy Information Administration. *Overview: Energy Trends to 2030*. 2007. December 11, 2007 <<http://www.eia.doe.gov/oiaf/aeo/pdf/overview.pdf>>.
- ² Massachusetts Institute of Technology (MIT). *The Future of Coal: an MIT Interdisciplinary Study*. 2007. May 7, 2007. <http://web.mit.edu/coal/The_Future_of_Coal.pdf>.
- ³ Energy Information Administration. *World Coal Markets*. 2006. May 7, 2007. <<http://www.eia.doe.gov/oiaf/ieo/pdf/coal.pdf>>.
- ⁴ US Environmental Protection Agency. Clean Air Mercury Rule. 2007. March 27, 2008. <<http://www.epa.gov/mercuryrule/>>.
- ⁵ Greenhouse, Linda. *Environmentalists Hail Supreme Court Ruling on Carbon*. 2007. May 7, 2007. <<http://www.iht.com/articles/2007/04/03/news/scotus.php>>.
- ⁶ Booras, George, Holt, Neville. Pulverized Coal and IGCC Plant Cost and Performance Estimates. Gasification Technologies. EPRI. 2004.
- ⁷ Rizeq, George, West, Janice. Fuel-Flexible Gasification-Combustion Technology for Production of H₂ and Sequestration-Ready CO₂ GE Global Research. 2003.
- ⁸ Stiegel, G.J., Maxwell, R.C. "Gasification technologies: The path to clean, affordable energy in the 21st century." Fuel Processing Technology. 71. 79-97. 2001.
- ⁹ Beychok, M.R. "Coal Gasification and the Phenosolvan Process." American Chemical Society, Division of Fuel Chemistry. 19.5. p168. National Meeting of American Chemical Society. 8 Sep 1974. Atlantic City, NJ.
- ¹⁰ Reinecke, Chris. "Coal and Gasifiers." Sasol. 2006. 29 Nov 2007 <http://sasol.investoreports.com/sasol_mm_2006/html/sasol_mm_2006_9.php>.
- ¹¹ Simento, Noel. "IGCC Power Generation." Cooperative Research Centre for Coal in Sustainable Development. 2002. 28 Nov 2007 <<http://www.ccsd.biz/factsheets/igcc.cfm>>.
- ¹² "Gasification: ConocoPhillips E-Gas Gasifier." NETL. 2007. 28 Nov 2007 <<http://www.netl.doe.gov/technologies/coalpower/gasification/pubs/photo.html>>.
- ¹³ Davey, William, Taylor, Edward, Larsen, Paul. Atmospheric Pressure, Entrained Flow, Coal Gasification Re-Visited. AECI, Kynoch Fertilizer Limited, Babcock and Wilcox. 2000.
- ¹⁴ Tavoulareas, E. Stratos, Charpentier, Jean-Pierre. "Clean Coal Technologies for Developing Countries," World Bank Technical Paper No. 286, Energy Series. July 1995. <<http://www.worldbank.org/html/fpd/em/power/EA/mitigatn/igccsubs.htm>>.
- ¹⁵ Helble, Joseph. "Trace Element Partitioning during Coal Gasification." Fuel. 75.8. 931-939. 1996.

-
- ¹⁶ McDaniel, John. Tampa Electric Polk Power Station Integrated Gasification Combined Cycle Project. NETL. 2002.
- ¹⁷ "Polk Power Station." Tampa Electric Company. 2007. 28 Nov 2007 <<http://www.tampaelectric.com/news/tri/summary/>>.
- ¹⁸ Geositls, Robert, Schmoe, Lee. "IGCC – The Challenges of Integration." Bechtel Corporation. ASME Turbo Expo 2005: Power for Land, Sea, and Air. June 6-9, 2005. Reno-Tahoe, NV.
- ¹⁹ "E-Gas in Action." ConocoPhillips. 2004. 28 Nov 2007 <<http://www.coptechnologysolutions.com/egas/action/index.htm>>.
- ²⁰ Nowak, Milton, and William Singer. "Mercury Compounds." Kirk-Othmer Encyclopedia of Chemical Technology. John Wiley & Sons, Inc, 1995. Gordon Library, Worcester. 6 Dec. 2007.
- ²¹ Devito, Stephen C., and William E. Brooks. "Mercury." Kirk-Othmer Encyclopedia of Chemical Technology. John Wiley & Sons, Inc., 2005. Gordon Library, Worcester. 6 Dec. 2007.
- ²² Smith, Mark. "Mercury Sources, Emission Monitoring, and Source Release Estimates." MassDEP. 8 Aug. 1996. MA DEP. 30 Dec. 2007. <<http://www.mass.gov/dep/toxics/stypes/hgch3b.htm>>.
- ²³ "Consumption Advice." U.S. Environmental Protection Agency. 19 July 2007. 7 Dec. 2007. <<http://www.epa.gov/waterscience/fishadvice/factsheet.html>>.
- ²⁴ "Consumer Factsheet on: Mercury." U.S. Environmental Protection Agency. 28 Nov. 2006. 6 Dec. 2007. <<http://www.epa.gov/safewater/dwh/c-ioc/mercury.html>>.
- ²⁵ "Arsenic in Drinking Water." U.S. Environmental Protection Agency. 26 Mar. 2007. 6 Dec. 2007. <<http://www.epa.gov/safewater/arsenic/basicinformation.html>>.
- ²⁶ "Arsenic Toxicity: Who is At Risk." Agency for Toxic Substances and Disease Registry. Oct. 2000. 7 Dec. 2007. <<http://www.atsdr.cdc.gov/csem/arsenic/whosatrisk.html#public>>.
- ²⁷ Doak, G O., G Long, and Leon D. Freedman. "Arsenic Compounds." Kirk-Othmer Encyclopedia of Chemical Technology. John Wiley & Sons, Inc, 2000. Gordon Library, Worcester. 6 Dec. 2007.
- ²⁸ "Consumer Factsheet on: Selenium." U.S. Environmental Protection Agency. 28 Nov. 2006. 6 Dec. 2007. <<http://www.epa.gov/safewater/dwh/c-ioc/selenium.html>>.
- ²⁹ "Selenium (Se) - Chemical Properties." LennTech. 1998. 7 Dec. 2007. <<http://www.lennotech.com/Periodic-chart-elements/Se-en.htm>>.
- ³⁰ Hoffmann, J E., and M G. King. "Selenium And Selenium Compounds." Kirk-Othmer Encyclopedia of Chemical Technology. John Wiley & Sons, Inc., 2001. Wiley InterScience. Gordon Library, Worcester. 6 Dec. 2007.

-
- ³¹ Ratafia-Brown, Jay, Stiegel, Gary. "An Environmental Assessment of IGCC Power Systems." DOE. Nineteenth Annual Pittsburg Coal Conference. Sept. 23-27, 2002.
- ³² Helsen, Lieve. "Sampling Technologies and Air Pollution Control Devices for Gaseous and Particulate Arsenic: A Review." Environmental Pollution. 137. 305-315. 2005.
- ³³ Lopez-Anton, M.A. "Retention of Arsenic and Selenium compounds present in Coal Combustion and Gasification Flue Gases using Activated Carbons." Fuel Processing Technology. 88. 799-805. 2007.
- ³⁴ Molina, Luis M., and Alonso, Julio A. "Chemical Properties of Small Au Clusters: An Analysis of the Local Site Reactivity". Journal of Physical Chemistry. 111. 6668-6677. 2007.
- ³⁵ Remediakis, Ioannis N., Lopez, Nuria, and Norskov, Jens K. "CO oxidation on gold nanoparticles: Theoretical Studies". Applied Catalysis A: General. 291.13-20. 2005.
- ³⁶ Alper, Charles N., Hunerlach, Michael P. *Mercury Contamination from Historic Gold Mining in California*. 2005. December 14, 2006. <<http://ca.water.usgs.gov/mercury/fs06100.html>>.
- ³⁷ Date, M., Imai, H., Tsubota, S., and Haruta, M. "In Situ measurements under flow condition of the CO oxidation over supported gold nanoparticles." Catalysis Today. 122. 222-225. 2007.
- ³⁸ Hwang, C.B, et al. "Synthesis, Characterization, and Highly Efficient Catalytic Reactivity of Suspended Palladium Nanoparticles." Journal of Catalysis. 195. 336-341. 2001.
- ³⁹ Narayanan, Radha, El-Sayed, Moftata. "Effect of Catalysis on the Stability of Metallic Nanoparticles: Suzuki Reaction Catalyzed by PVP-Palladium Nanoparticles." Journal of the American Chemical Society. 125. 8340-8347. 2003.
- ⁴⁰ Kim, Sang-Wook et al. "Synthesis of Monodisperse Palladium Nanoparticles." Nano Letters. 3.9. 1289-1291. 2003.
- ⁴¹ Wang, C.C, Chen, D.H., Huang, T.C. "Synthesis of palladium nanoparticles in water-in-oil microemulsions." Colloids and Surfaces. 189. 145-154. 2001.
- ⁴² Takeda, Norihiko, et al. "Effect of Inert Supports for Titanium Dioxide Loading on Enhancement of Photodecomposition Rate of Gaseous Propionaldehyde." Journal of Physical Chemistry. 99. 9986-9991. 1995.
- ⁴³ "Nanoparticles." American Elements. 2008. 12 Feb 2008. <http://www.americanelements.com/Submicron_nano_powders.htm>.
- ⁴⁴ Diaz, E, Ordonez, S,Vega, A, Coca, J. "Adsorption properties of a Pd/ γ -Al₂O₃ catalyst using inverse gas chromatography." Microporous and Mesoporous Materials. 70. 109-118. 2004.

-
- ⁴⁵ McGown, William et al. "Hydrogenation of acetylene in excess ethylene on an alumina supported palladium catalyst in a static system." Journal of Chemical Society, Faraday Transitions. 1.73. 632-647. 1977.
- ⁴⁶ Ihm, Sun, Lee, Dong. "Process for manufacturing a titania supported palladium catalyst." US Patent 4839329. Oct. 23, 1987.
- ⁴⁷ Clark, James et al. "Preparation of a novel silica-supported palladium catalyst and its use in the Heck reaction." Green Chemistry. 2. 53-56. 2000.
- ⁴⁸ Youquan Deng, F.S. et al. "A novel ZrO₂-SO₄⁻² supported palladium catalyst for syntheses of disubstituted ureas from amines by oxidation carbonylation." Tetrahedron Letters. 42.11. 2161-2163. 2001.
- ⁴⁹ Li, Wenzhen, et al. "Carbon Nanotubes as support for cathode catalyst of a direct methanol fuel cell." Letters to the Editor/Carbon. 40. 791-794. 2002.
- ⁵⁰ Granger, P et al. "Kinetics of the NO and CO Reaction over Platinum Catalysts." Journal of Catalysis. 173. 304-314. 1998.
- ⁵¹ Mizukoshi, Yoshiteru, et al. "Preparation of Platinum Nanoparticles by Sonochemical Reduction of the Pt(II) Ion." Langmuir. 15. 2733-2737. 1999.
- ⁵² Joo, Sang Hoon, et al. "Ordered nanoporous arrays of carbon supporting high dispersions of platinum nanoparticles." Nature. 412. 169-173. 2001.
- ⁵³ Ingelsten, H.H et al. "Deposition of Platinum Nanoparticle, Synthesized in Water-in-Oil Microemulsions, on Alumina Supports." Langmuir. 18. 1811-1818. 2002.
- ⁵⁴ Prado-Burguette, C. et al. "Effect of carbon support and mean Pt particle size on hydrogen chemisorption by carbon-supported Pt catalysts." Journal of Catalysis. 128. 397-404. 1991.
- ⁵⁵ Bozo, Christine et al. "Role of the Ceria-Zirconia Support in the Reactivity of Platinum and Palladium Catalysts for Methane Total Oxidation under Lean conditions." Journal of Catalysis. 203. 393-406. 2001.
- ⁵⁶ Yoshitake, Hideaki, Iwasawa, Yasuhrio. "Electronic Metal-Support Interaction in Pt Catalysts under Deuterium-Ethene Reaction Conditions and the Microscopic Nature of the Active Sites." Journal of Physical Chemistry. 96. 1329-1334. 1992.
- ⁵⁷ Mineral Isolation Institute. *Vanadium*. December 11, 2007. <<http://www.mii.org/Minerals/photovan.html>>.
- ⁵⁸ IEA Clean Coal Centre. "Clean Coal Technologies: Selective catalytic reduction (SCR) for NO_x control." February 15, 2008. <<http://www.ied-coal.org.uk/content/default.asp?PageId=999>>.
- ⁵⁹ MECS. (2002) *Catalyst Poisoning or Deactivation*. December 11, 2007. <<http://www.mecsglobal.com/MECS/images/Brochures/Catalyst/CatalystPoisoningOr>>.

Deactivation-2002.pdf>.

⁶⁰ Waldrop, Mitchell. "Nanoscale Iron Could Help Cleanse the Environment." National Science Foundation. 3 Sept. 2003. 10 Dec. 2007. <http://www.eurekalert.org/pub_releases/2003-09/nsf-nic090303.php>.

⁶¹ "Scientists Find Benefits in Using Some Types of Iron Nanoparticles for Environmental Clean-Up." AZoNanoparticles. 12 Jan. 2005. 7 Dec. 2007. <<http://www.azonano.com/details.asp?ArticleID=1161>>.

⁶² Borchardt, John K. "Nanotech Shows Promise for Cheaper Superfund Cleanup." USA Today. 10 Feb. 2005. The Christian Science Monitor. 5 Dec. 2007. <http://www.usatoday.com/tech/news/nano/2005-02-10-nano-iron-cleanup_x.htm>.

⁶³ Minchev, C., Huwe, H., Tsoncheva, T., Paneva, D., Dimitrov, M., Mitov, I., and Froba, M. "Iron Oxide Modified Mesoporous Carbons: Physicochemical and Catalytic Study." Microporous and Mesoporous Materials. 81. 333-341. 2005.

⁶⁴ Wolf, A, A Lange De Oliveira, C Kiener, R Brinkmann, H Bonnemann, and F Schuth. "Supported Catalysts: Copper, Silver & Gold on Transition Metal Oxides." Max-Planck-Institute fu Kohlenforschung, Mulheim an Der Ruhr. 6 Dec. 2007 <http://www.kofo.mpg.de/kofo/institut/arbeitsbereiche/schueth/pdf_poster/sc_cat.pdf>.

⁶⁵ DOE/Brookhaven National Laboratory. "Gold, Copper Nanoparticles Take Center Stage In The Search For Hydrogen Production Catalysts." ScienceDaily 29 March 2007. 7 December 2007. <<http://www.sciencedaily.com/releases/2007/03/070328111145.htm>>.

⁶⁶ Kitco, Inc. 2007. 27 Jan. 2008. <<http://www.kitco.com/market/>>.

⁶⁷ Lischka, Hans, Holger Dachsel, Ron Shepard, and Robert J. Harrison. "Parallel Computing in Quantum Chemistry-Message Passing and Beyond for a General Ab Initio Program Study." High Performance Computing and Networking. 203-209. 1994.

⁶⁸ "Product Information." Gaussian 03W. 2007. 3 Dec. 2007 <gaussian.com>. Profeta, Salvatore. "Molecular Modeling." Kirk-Othmer Encyclopedia of Chemical Technology 16. 726-765. 2005.

⁶⁹ McCormack, J M., and M C. Nagan. "Molecular Modeling 2: Computational Chemistry." 27 Feb. 2007. 3 Dec. 2007. <<http://chemlab.truman.edu/CHEM121Labs/MolecularModeling2.htm>>.

⁷⁰ "Gaussian 03 Online Manual." Gaussian.Com. 2 Oct. 2006. 3 Dec. 2007. <http://gaussian.com/g_ur/m_basis_sets.htm>.

⁷¹ "Ab Initio Methods." 23 May 2006. Department of Chemistry, University of Maine. 3 Dec. 2007. <<http://chemistry.umeche.maine.edu/Modeling/abinit.html>>.

-
- ⁷² Check, Catherine E., Timothy O. Faust, John M. Bailey, Brian J. Wright, Thomas M. Gilbert, and Lee S. Sunderlin. "Addition of Polarization and Diffuse Functions to the LANL2DZ Basis Set for P-Block Elements." Journal of Physical Chemistry A. 105. 34. 8111 -8116. 2001.
- ⁷³ Bartlett, Rodney J. Recent Advances in Coupled Cluster Methods. Vol. 3. World Scientific, 1997. 12 Feb. 2008. <<http://books.google.com/books?id=81RLqhJ09C4C&pg=PA242&lpg=PA242&dq=qcis+doubles+excitations&source=web&ots=DRwL8dsdbz&sig=Z7efsleEnuLV0q0RDt76iB4a5w4#PPA242,M1>>.
- ⁷⁴ "Multiplicity (Spin Multiplicity)." IUPAC Compendium of Chemical Technology. 1997. 8 Jan. 2008.
- ⁷⁵ Steckel, Jan. "Computational Approaches to the Development of Advanced Mercury Control Technologies." National Energy Technology Laboratory. February 25, 2008. <<http://www.netl.doe.gov/publications/proceedings/04/HgReview/2004HgSteckel.pdf>>.
- ⁷⁶ Fernandez, L.E. and Varetti, E.L. "Computational note on the quantum chemistry calculated force constants of the CF₃SeX (X=H, D, Cl, Br) molecules." Journal of Molecular Simulation. 761. 217. 2006.
- ⁷⁷ Ho, J., Polak, M.L., Ervin, K.M., Lineberger, W.C. Journal of Chemical Physics. 99. 8542. 1993.
- ⁷⁸ - Kordis, J., Gingerich, K.A., Seyes, R.J. Journal of Chemical Physics. 61. 5114. 1974.
- ⁷⁹ Gupta, S.K., Nappi, B.M., Gingerich, K.A. Inorganic Chemistry. 20. 966. 1981.
- ⁸⁰ Gronbeck, H., Rosen, A. Journal of Chemical Physics. 107. 10620. 1997.
- ⁸¹ Leopold, D.G., Ho, J., Lineberger, W.C. Journal of Chemical Physics. 86. 1715. 1987.
- ⁸² De Vore, T.C., Ewing, A., Franzen, H.F., Calder, V. Chemical Physics Letters. 35. 78. 1975.
- ⁸³ Purdum, H., Montano, P.A., Shenoy, G.K., Morrison, T. Physics Review B. 25. 4412. 1982.
- ⁸⁴ "2.2 How Do Molecules Bond to Surfaces?" Queen Mary, University of London. 1 Feb. 2008 <http://www.chem.qmul.ac.uk/surfaces/scc/scat2_2.htm>.
- ⁸⁵ Hudson, John. "Gas-Surface Interactions." Surface Science: an Introduction. Wiley-IEEE: 1998. 25 Feb. 2008. <http://books.google.com/books?id=TTPMbOGqFYC&pg=PA178&lpg=PA178&dq=chemisorption,+1015+kcal/mol&source=web&ots=J6BhYRo_nY&sig=_xnayaq5CaSuI5WS7cEOP60O6p8#PPA178,M1>.

⁸⁶ Nasri, N.S., Jones, J.M., Dupont, V.A., Williams, A. "A Comparative Study of Sulfur Poisoning and Regeneration of Precious-Metal Catalysts" Energy & Fuels. 12. 1130-1134. 1998.

⁸⁷ Arabczyk, W., Narkiewicz, U., Moszynski, D. "Chlorine as a poison of the fused iron catalyst for ammonia synthesis." Applied Catalysis A: General. 134. 2. 331-338. 1996.